ELSEVIER

International Journal of Mass Spectrometry 214 (2002) 129–154

International Journal of Mass Spectrometry

www.elsevier.com/locate/ijms

Dissociation behavior of ionized valeramide Part II. Theoretical exploration of the potential-energy surface

Marija Semialjac, Jessica Loos, Detlef Schröder*, Helmut Schwarz

Institut für Chemie der Technischen Universität Berlin, Strasse des 17, Juni 135, D-10623 Berlin, Germany

Received 23 November 2001; accepted 3 December 2001

Abstract

The ionization of valeramide and the subsequent rearrangements and fragmentations of the cation radical are studied by quantum-chemical calculations employing the B3LYP method, while molecular modeling techniques are used for an initial screening of the conformational space. Ionization of valeramide involves a modest difference between adiabatic and vertical ionization energies. Interestingly, the cation radical bears several, rather low-lying routes for unimolecular rearrangements. The energetically preferred route involves initial γ-C–H bond activation according to the well-known McLafferty rearrangement. Other, low-lying channels proceed via β-C–H and δ-C–H bond activations, respectively, leading to specific fragmentation reactions which are analyzed in detail. Further, direct β-C–C bond cleavage of ionized valeramide is explored. The theoretical results agree quite nicely with the experimental data presented in the preceding article as far as the relative energetic ordering of the fragmentation channels, isotope effects, and the occurrence of H/D equilibration are concerned. However, the calculations do not provide a straightforward mechanistic rationale for the experimentally observed variations in the branching ratios. (Int J Mass Spectrom 214 (2002) 129–154) © 2002 Elsevier Science B.V. All rights reserved.

Keywords: B3LYP calculations; C–H bond activation; Cation radicals; Rearrangements; Valeramide

1. Introduction

The paramount importance of amides for living organisms has stimulated experimental research followed by theoretical investigations on the physical properties of the peptide bond. Structural studies of small amides aid in a better understanding of peptide bonds in biological molecules. Our main interest in the subject of amides concerns the reaction mechanisms of amide rearrangements upon chemical activation, electron transfer in particular, which might hopefully lead to a better understanding of biological systems. As a model molecule, we have chosen ionized valeramide, a relatively small amide with a chain of five carbon atoms, which may mimic the behavior of larger amides. The theoretical results reported here are complemented by the preceding paper on experimental studies of ionized valeramide [1] and the subsequent paper [2] which summarizes the results, resolves the remaining differences and exploits the consequences for the interpretation of mass spectra of carbonyl compounds in a more general sense.

* Corresponding author. E-mail: df@www.chem..tu-berlin.de

1387-3806/02/$20.00
PII S1387-3806(01)00585-1

2. Computational methods

Most calculations were performed with the GAUSSIAN 98 suite of programs [3]. The use of density functional theory (DFT) was a natural choice because of the balance between accuracy and computational costs. The B3LYP functional which is a HF/DFT hybrid combining Becke's three-parameter semi-empirical exchange functional (B3 [4]) with the Lee–Yang–Parr correlation functional (LYP [5]) was used throughout. It should be mentioned that the B3LYP functional implemented in the GAUSSIAN program is slightly different than the original formula suggested by Becke, but since the method is actually semi-empirical, it cannot be claimed that one or another form of the functional is clearly superior to another [6]. Geometry optimizations were performed with Pople's polarized double-ζ 6-31G∗ basis set. For the sake of brevity, we refrain from an explicit discussion of all geometrical features of the various isomers examined as well as their conformers. The complete structures are given as Cartesian coordinates in Appendix A.

In order to characterize the optimized structures, frequency analysis has been performed at the same level of theory. Minima were characterized by the absence of imaginary vibrational modes, while the transition structures involved one imaginary frequency. Reaction pathways have been followed by IRC calculations at the same level of theory. Because the B3LYP/6-31G∗ calculations overestimate force constants, the zero-point energies (ZPEs) obtained at this level were scaled by 0.9805, which is the average of the factors proposed by Scott and Radom [7] and Wong [8]. The scaled ZPEs were subsequently used in the conversion of electronic energies to relative energies at 0 K. Further, the computed parameters were used to determine the relative energetics at 298 K in order to acknowledge thermal contributions in ion dissociation, where the GAUSSIAN program uses unscaled frequencies in this formalism. In order to get more reliable energetic profiles of the reactions in question, single point calculations using triple-ζ basis sets with diffuse functions included (6-311++G∗∗) were performed. Thus, relative energies of the stationary points were calculated at the B3LYP/6-311++G∗∗//B3LYP/6-31G∗ level of theory, where the ZPEs calculated with B3LYP/6-31G∗ were used in the conversion to relative energies at 0 K.

Further, an initial screening of the conformational space of valeramide was performed with the MM2 method implemented in the Spartan program [9].

3. Results and discussion

3.1. Computational approach

As far as a viable computational approach to the potential-energy surface (PES) of ionized valeramide is concerned, several problems have to be dealt with and a reasonable compromise had to be reached. Thus, valeramide is already quite a large molecule for advanced ab initio methods, and moreover, the distonic ions formed as reaction intermediates demand for a proper description of electron correlation. Further, valeramide, being it neutral or charged, is a rather flexible system for which a large number of energetically low-lying conformers may contribute to the chemistry observed at ambient temperature.

Superimposed to these more general aspect is a specific problem of amides which concerns the rotation around the C–N bond. Therefore, a brief survey about previous theoretical studies of amides is indicated. Formamide, the smallest amide, has been widely studied both experimentally and theoretically. The main interest has been focused on the planarity of the NH_2 group [10]. The microwave spectrum of formamide [11] is consistent with an inversion potential for the NH_2 group with a very shallow minimum for a non-planar structure. However, earlier experimental investigations have suggested the presence of a planar amide unit both in the gas phase and in the solid state of formamide as well as substituted amides [12–14]. While a large number of theoretical calculations has been carried out on model amides, the results are controversial [15]. Moreover, the solvents present in biological systems may substantially influence the

abundance of non-planar (chiral) amides [16]. Contradictory results have been published for the conformational minima of acetamide, which can essentially assume three different types of conformations: *syn*, perpendicular, and *anti*, where we follow the terminology proposed by Samdal [17]. B3LYP/6-311++G** and B3LYP/cc-pVTZ calculations suggest that the *anti*-conformer is most stable. Helgaker et al. [18] have tested several computational methods with different basis sets for the equilibrium structures of small molecules. In these tests, the MP2/cc-pVTZ level of theory gave a very good agreement with the experimentally obtained equilibrium geometries. However, there is still an open question whether those methods can predict correct conformational minima and barrier heights as well. Thus, in the case of acetamide MP2/cc-pVTZ calculations predict a second stable conformational minimum, which is of a perpendicular form with the torsional angle of 30°. The energy difference between the *anti* and perpendicular structures amounts to only 3 cal/mol. Samdal tried and failed to locate the transition structure (TS) connecting these two conformers with conventional methods of geometry optimization [17]. For this reason, a calculation at a fixed geometry (torsional angle of 45°) mimicking the transition structure has been performed and the barrier has been estimated at about 4 cal/mol. In an extensive conformational study on acetamide, Wong and Wiberg found perpendicular conformation to be the most stable one when MP2 and CISD methods were used [19]. In summary, the methods employed so far cannot give a clear answer whether the *anti* or perpendicular conformation is the most stable one.

For an extensive ab initio study, valeramide is a relatively large molecule, thereby imposing some restrictions to the computational approach applicable. Moreover, several conformers have to be considered of which each might give rise to particularly favorable pathways. An appropriate computational description of ionized valeramide and of its rearrangement reactions requires, however, a reasonably solid quantum chemical approach which is able to adequately describe closed- and open-shell species, electron delocalization, hydrogen bonding, and transition structures in particular. In these respects, DFT is very successful in predicting physical properties of molecular systems, including hydrogen-bonded species, with an accuracy equal or even better than obtained by MP2 calculations [20,21], but at much lower computational costs than higher levels of theory [22]. The present choice of B3LYP/6-311++G**//B3LYP/6-31G* is therefore, considered as a proper level of theory to gain reliable potential-energy surfaces [6]. In turn, however, the computations at this level are already quite demanding such that the potential-energy surface of ionized valeramide cannot be explored exhaustively. Therefore, the theoretical examination was primarily guided by the mechanistic implications derived from the experimental studies [1] in conjunction with chemical intuition and plausibility considerations as far as the choice of low-lying conformations is concerned. As far as the description of the distonic ion intermediates is concerned, the B3LYP/6-31G* geometries appear to suffice, since complete geometry optimizations of a few key species at the B3LYP/6-311++G** level of theory did not show large differences between the two methods neither in geometrical parameters nor in energetics. Accordingly, full geometry optimizations of all species were not performed at this level because the quality of the results would not change while the computational costs would increase considerably. Of course, it is admitted frankly that the computational approach chosen does not ensure that all relevant conformers were covered. Nevertheless, the reasonable agreement between theory and experiment obtained after all justifies our pragmatic choice of the theoretical approach.

3.2. Conformational analysis of neutral and ionized valeramide

As one can infer from the work done so far on formamide and acetamide (see above), conformational analysis can be quite demanding even for smallest amides. If we now turn to valeramide as the subject of this study, it is clear that the situation is even more complex. By analogy to the three leading conformers proposed for acetamide, one can postulate the

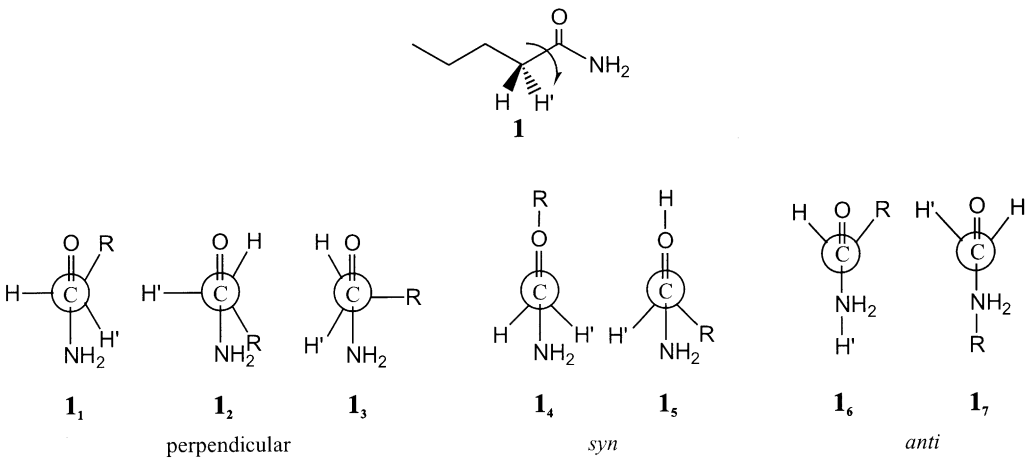

Fig. 1. Newman projections along the C(1)–C(2) bond of valeramide showing the possible conformations of the amide group.

existence of seven conformational minima for valeramide (Fig. 1) which differ with respect to the orientations of the substitutents at C(1) and C(2). In addition, the alkyl chain of valeramide may adopt several conformations. In combination with the different functional group orientations, a considerable number of energetically low-lying conformers evolves. For an initial screening, conformational analysis of valeramide was performed with conformational search algorithm of the MM2 force field. More than 70 conformers were obtained within the energy range of only 3 kcal/mol. Accordingly, a manifold of conformers is expected to be sampled in experimental studies conducted at or above room temperature. For such a large number of possible conformers, an explicit consideration of all MM2 structures on the B3LYP level of theory is not practical. We are mostly interested in different orientations of the functional group, and thus only those conformers were fully optimized at the B3LYP level of theory (Fig. 1), while the alkyl backbone was confined to an *all-anti*-conformation. Interestingly, the most stable conformer obtained in the MM2 calculations (similar to $\mathbf{1_5}$) does not even exist on the B3LYP surface, which can be attributed to the failure of molecular mechanics to describe reliably hydrogen- and weak-bond interactions. On the B3LYP level of theory, only two different conformations, $\mathbf{1_1}$ and $\mathbf{1_2}$, both belonging to the perpendicular case, were located; the latter is less stable due to steric repulsion between R and the amino group. Geometry optimizations for all the other possibilities ended in structure $\mathbf{1_1}$, suggesting it as the global conformational minimum. The failure to locate the other conformations does, however, not explicitly indicate that these conformers do not exist as minima on the PES of valeramide. Therefore, a PES scan was performed keeping the dihedral angle θ_{CCCO} fixed while freely optimizing all other parameters. The results of the scan are consistent with structure $\mathbf{1_1}$ as the global minimum (Table 1). The energy increase that accompanies the changes in the dihedral angle can be explained by contributions of at least two factors: (i) steric repulsion between the alkyl unit ($CH_3CH_2CH_2$) and the amino group (basically hydrogen repulsions), and (ii) stabilization caused by the interaction of one of the C(2) hydrogens with the p_π-orbital on C(1), which compensates the positive charge emerging from the polarized bonds to the heteroatom substituents of C(1). The latter stabilization is most pronounced in the perpendicular conformations in which the interacting hydrogen atom forms a dihedron θ_{HCCO} of approximately 90°, thereby maximizing orbital overlap. Energetic preference of this interaction also explains why only the perpendicular conformers

Table 1
Energetics derived from a scan of the dihedral angle θ_{CCCO} in neutral valeramide[a,b] at the B3LYP/6-31G* level of theory

Conformer[c]	θ_{CCCO}[b]	E_{tot}[d]	E_{rel}[e]
1₄	0	−327.15421	0.11
1₁	30	−327.15439	0.00
1₆	60	−327.15393	0.29
1₃	90	−327.15302	0.86
1₅	120	−327.15246	1.21
1₂	150	−327.15224	1.35
1₇	180	−327.15222	1.36

[a] In these calculations, θ_{CCCO} was kept fixed, while all other parameters were fully optimized.
[b] Specifically, this is the dihedral angle spanned by the atoms O, C(1), C(2), and C(3).
[c] See Fig. 1.
[d] Total energies in Hartree; $1H = 627.51$ kcal/mol.
[e] Energies (kcal/mol) relative to the most stable conformer **1₁**.

1₁ and **1₂** exists as minima at the B3LYP level of theory.

Because our interest concerns the further rearrangements of valeramide cation-radical, rather than locating all possible conformers of either neutral or cationic valeramide, structure **1₁** was chosen as a general reference point. Nevertheless, the ambiguities about the conformational minima of valeramide as well as other amides (see above) cast some doubt on the quantitative aspects of the present analysis because we cannot a priori exclude that other, hitherto not considered conformers contribute to the chemistry of the ionic species.

3.3. Adiabatic and vertical ionization of valeramide

Adiabatic and vertical ionization energies (IE_a and IE_v) were calculated for the conformers **1₁** and **1₂** of neutral valeramide (Table 2) [23]. However, geometry optimizations on the cation-radical PES leads to the same cation structure $\mathbf{1_1}^{+\bullet}$ for both conformers; note that the conformational indices used for neutral and ionized valeramide do not coincide. The difference between vertical and adiabatic ionization ($\Delta IE_{v/a}$) is 0.36 eV for conformer **1₁** and 0.28 eV for conformer **1₂**, indicating that the structural changes upon ionization are slightly more pronounced in the former. With regard to the experimentally obtained ionization energy ($IE = 9.40 \pm 0.03$ eV), the relatively small $\Delta IE_{v/a}$ implies that the onset for photoionization of valeramide corresponds to adiabatic ionization. Further, the energy difference of the conformers **1₁** and **1₂** is small, such that mixtures of at least these two conformers are likely to be sampled in the experiments. The calculated energetic difference of ∼1 kcal/mol suggests a ca. 5:1 ratio of **1₁** and **1₂** at 298 K. Nevertheless, due to the similarity of the computed adiabatic and vertical IEs, the presence of a mixture may safely be neglected in comparing the experimental and theoretical data. Relative to experiment, one notes a slight underestimation of the adiabatic IEs, which may be attributed to a general trend of the B3LYP approach in predicting IEs of closed-shell organic molecules [24,25]. Upon ionization, geometry changes from the perpendicular into the distorted *anti*-conformation (Fig. 2), similar to conformer **1₅** of neutral valeramide, with the dihedral angles $\theta_{RCCO} = 46.3^\circ$ and $\theta_{HCCO} = 13.2^\circ$. In the cation radical, the electron deficient oxygen atom orientates in such a manner that the stabilization through bond delocalization from neighboring NH_2- and CH_2-groups can occur, which is reflected

Table 2
Relative stabilities (E_{rel} in kcal/mol) of valeramide conformers, their calculated adiabatic and vertical ionization energies (IE_a and IE_v, respectively, in eV)[a] and their difference $\Delta IE_{v/a}$ (eV)

Conformer	Method	E_{rel}	IE_a	IE_v	$\Delta IE_{v/a}$
1₁	B3LYP/6-31G*//B3LYP/6-31G*	0.0	8.88	9.24	0.36
	B3LYP/6-311++G**//B3LYP/6-31G*	0.0	9.19	9.55	0.36
1₂	B3LYP/6-31G*//B3LYP/6-31G*	1.4	8.82	9.10	0.28
	B3LYP/6-311++G**//B3LYP/6-31G*	1.0	9.15	9.43	0.28

[a] Note that adiabatic ionization of both conformers of neutral valeramide leads to the same structure for the ion (see text).

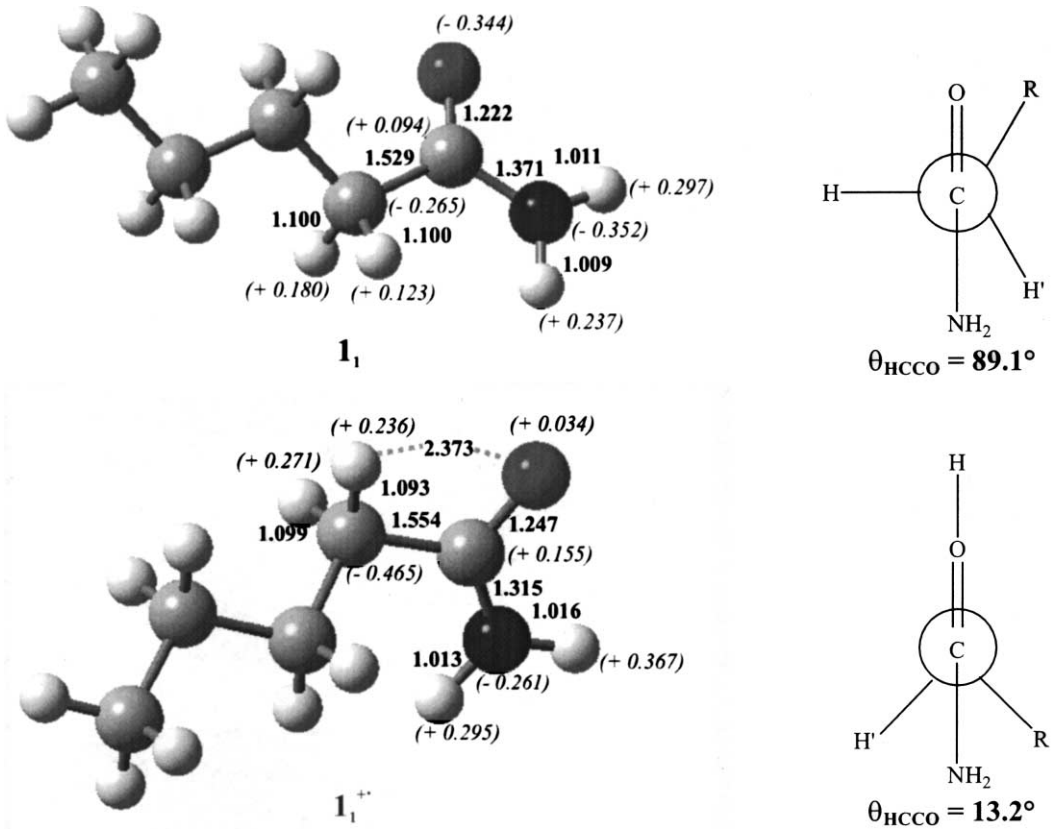

Fig. 2. Optimized structures of neutral and ionized valeramide at the B3LYP/6-31G∗ level of theory. Bond lengths (Å) are given in bold, Mulliken charges in parentheses.

in the changes of the charge distributions for neutral and ionized valeramide. Consideration of the molecular orbitals supports this picture in that the cationic species bears orbitals which are delocalized across the C–H and N–H bonds and the carbonyl group. The changes in dihedral angles are the main cause of the difference between adiabatic and vertical ionization, while bond angles and bond lengths experience only minor variations. The elongation of the C(1)–C(2) bond, e.g., is rather small with r_{CC} = 1.529 Å in the neutral compared to r_{CC} = 1.554 Å in the cation radical. Concerning the planarity of amino group, the already almost planar arrangement in the neutral (the sum of the angles around nitrogen is 358°) becomes perfect in the cation radical $\mathbf{1_1}^{+\bullet}$ due to better overlap between orbitals including the N–H bonds and the oxygen atom.

3.4. Unimolecular dissociations of ionized valeramide

Detailed reaction pathways have been calculated for the five fragmentation channels of ionized valeramide deduced from the experimental studies (Scheme 1). For the sake of consistency, the notations of the various intermediates and products used in [1] are adopted throughout. The C_3-route corresponds to the McLafferty rearrangement which is initiated by 1,5-hydrogen transfer and followed by C–C bond cleavage and expulsion of propene con-

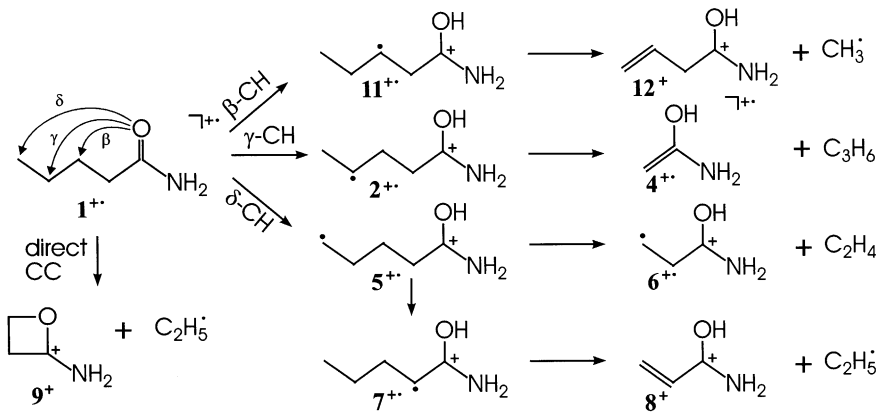

Scheme 1.

comitant with formation of the enol cation $\mathbf{4}^{+\bullet}$. The C_2-route comprises three channels. Two of these have initial 1,6-hydrogen transfer in common, i.e., the loss of C_2H_4 to afford the β-distonic ion $\mathbf{6}^{+\bullet}$ and the indirect loss of $C_2H_5^{\bullet}$ to form protonated acrylamide $\mathbf{8}^{+}$ in a more complex process. The third contributor to the C_2-route is the direct loss of the terminal ethyl group in which the main concern is the structure of the associated product ion; this problem is postponed to the discussion of the exit channels. Based on the experimental findings, the C_1-route is assigned to an initial 1,4-hydrogen transfer followed by loss of $CH_3^{\bullet}$ concomitant with formation of protonated vinylacetamide $\mathbf{12}^{+}$. Finally, even though occurrence of 1,3-hydrogen transfer, viz. keto/enol tautomerization, has not been inferred from experiment, it was included in the theoretical study as well.

In perfect agreement with the interpretation of the experimental data, the barriers associated with the various hydrogen migrations in the cation radical are rather small. Accordingly, internal rotations around the C–C bonds play an important role in that adequate conformers need to be accessed before a particular rearrangement can occur. In fact, C–C bond rotations may contribute to or even essentially constitute the rate-determining steps. The structural flexibility of valeramide and its cation radical makes the mechanistic study rather demanding because the rearrangements could arise from many different conformers. As a compromise between insight gained and computational resources available, the role of internal rotations prior to hydrogen migration was only investigated explicitly for the C_2- and C_3-routes.

3.4.1. γ-C–H bond activation (C_3-route)

In the lowest-lying conformer $\mathbf{1_1}^{+\bullet}$, the distances between the oxygen atom of the carbonyl group and the hydrogens at C(4) are much too large for hydrogen migration. Rotation around the C(2)–C(3) bond leads to conformer $\mathbf{1_3}^{+\bullet}$ which is 1.5 kcal/mol higher in energy than $\mathbf{1_1}^{+\bullet}$ (Table 3). Although the absence of imaginary modes characterizes $\mathbf{1_3}^{+\bullet}$ as a real minimum at the B3LYP/6-31G∗ level of theory, all attempts failed to locate a barrier associated with hydrogen migration to the distonic ion $\mathbf{2}^{+\bullet}$ (Fig. 3). Moreover, all computed points of a continuous scan from $\mathbf{1_3}^{+\bullet}$ to $\mathbf{2}^{+\bullet}$, i.e., decreasing r_{OH} while optimizing all other parameters, were lower in energy than the starting point $\mathbf{1_3}^{+\bullet}$. Accordingly, the barrier associated with 1,5-hydrogen migration is rather small, if not spurious. Inspection of the computed vibrational frequencies reveals a low-lying mode at 89 cm^{-1} of $\mathbf{1_3}^{+\bullet}$ which reflects the structural changes associated with γ-C–H bond activation (Fig. 4).[1] Further

[1] The absence of imaginary modes in $\mathbf{1_3}^{+\bullet}$ may also result as an artifact of the limited size of the grid used in the B3LYP calculations.

Table 3
Electronic energies (E_{tot}, in Hartree), zero-point energies (ZPE, in Hartree), and relative energies (E_{rel}, in kcal/mol)[a] of the stationary points on the potential-energy surface of ionized valeramide

	B3LYP/6-31G*//B3LYP/6-31G*			B3LYP/6-311++G**//B3LYP/6-31G*	
	E_{tot}	ZPE	E_{rel}[b]	E_{tot}	E_{rel}[b,c]
$\mathbf{1_1}^{+\bullet}$	−326.827971	0.158796	0.0	−326.923706[d]	0.0
$\mathbf{1_1}^{+\bullet}/\mathbf{1_2}^{+\bullet}$	−326.823143	0.158583	2.9	−326.919235	2.7
$\mathbf{1_2}^{+\bullet}$	−326.826593	0.158765	0.9	−326.922514	0.8
$\mathbf{1_1}^{+\bullet}/\mathbf{1_3}^{+\bullet}$	−326.821654	0.158462	3.8	−326.917911	3.5
$\mathbf{1_3}^{+\bullet}$	−326.825397	0.158764	1.6	−326.921404	1.5
$\mathbf{1_2}^{+\bullet}/\mathbf{1_4}^{+\bullet}$	−326.821097	0.158601	4.2	−326.917217	4.0
$\mathbf{1_4}^{+\bullet}$	−326.824067	0.158917	2.6	−326.919870	2.5
$\mathbf{2}^{+\bullet}$	−326.851066	0.159234	−14.2	−326.952177	−17.6
$\mathbf{1_4}^{+\bullet}/\mathbf{5_1}^{+\bullet}$	−326.821475	0.158147	3.7	−326.917193	3.7
$\mathbf{5_1}^{+\bullet}$	−326.843174	0.159341	−9.2	−326.944120[d]	−12.4
$\mathbf{5_2}^{+\bullet}$	−326.831062	0.159672	−1.4	−326.933011	−5.3
$\mathbf{5_3}^{+\bullet}$	−326.829377	0.158749	−0.9	−326.932492	−5.5
$\mathbf{5_4}^{+\bullet}$	−326.827160	0.158382	0.3	−326.930411	−4.4
$\mathbf{5_1}^{+\bullet}$/c-$\mathbf{5}^{+\bullet}$	−326.819366	0.159789	6.0	−326.920266	2.8
c-$\mathbf{5}^{+\bullet}$	−326.821732	0.159752	4.5	−326.922196	1.6
$\mathbf{5_1}^{+\bullet}/\mathbf{6}^{+\bullet}$[e]	−326.795501	0.155755	18.5	−326.899203	13.5
$\mathbf{5_3}^{+\bullet}/\mathbf{7_1}^{+\bullet}$	−326.809434	0.155427	9.6	−326.912865	4.8
$\mathbf{7_1}^{+\bullet}$[f]	−326.851625	0.159665	−14.3	−326.954016	−18.5
$\mathbf{5_2}^{+\bullet}/\mathbf{7_2}^{+\bullet}$	−326.805264	0.155389	12.2	−326.908727	7.3
$\mathbf{7_2}^{+\bullet}$	−326.849834	0.159679	−13.1	−326.952205	−17.3
$\mathbf{1_1}^{+\bullet}/\mathbf{7_3}^{+\bullet}$	−326.782132	0.154218	26.0	−326.882266	23.2
$\mathbf{7_3}^{+\bullet}$	−326.854846	0.159999	−16.1	−326.957217	−20.3
$\mathbf{1_1}^{+\bullet}/\mathbf{1_1}^{+\bullet}$	−326.819324	0.154831	3.0	−326.916779	1.9
$\mathbf{1_1}^{+\bullet}$	−326.843288	0.159169	−9.4	−326.945129	−13.2
$\mathbf{1_1}^{+\bullet}/\mathbf{12}^{+}$[e]	−326.793115	0.155093	19.6	−326.897284	14.3

[a] The lowest-lying conformer $\mathbf{1_1}^{+\bullet}$ of the cation radical is used as the reference point.
[b] ZPEs included with a scaling factor of 0.9805.
[c] ZPEs taken from the B3LYP/6-31G*//B3LYP/6-31G* calculations.
[d] Energies at B3LYP/6-311++G**//B3LYP/6-311++G**: $\mathbf{1}^{+\bullet}$, −326.923857, and $\mathbf{5_1}^{+\bullet}$, −326.9442407.
[e] Barrier in the exit channel (see text).
[f] Computed energies of neutral **7**: E_{tot}(B3LYP/6-31G*) = −327.106796*H*, ZPE = 0.159554*H*, E_{tot}(B3LYP/6-311++G**//B3LYP/6-31G*) = −327.221313*H*.

refinement might certainly be achieved with larger basis sets in the geometry optimization combined with the application of tighter convergence criteria. With regard to the interpretation of the experimental data, however, it is entirely sufficient that the conformational barrier associated with the formation of $\mathbf{1_3}^{+\bullet}$ is predicted to exceed the kinetic restriction imposed by hydrogen migration. Hence, not C–H bond activation, but access to the appropriate conformation of $\mathbf{1}^{+\bullet}$ is rate-determining for the McLafferty rearrangement. This conclusion also provides an explanation for the negligible kinetic isotope effect (KIE) in the McLafferty route as derived from the analysis of the experimental data [1]. The distonic ion $\mathbf{2}^{+\bullet}$ is 17.6 kcal/mol more stable than the lowest-lying conformer of the reactant, $\mathbf{1_1}^{+\bullet}$. Bond lengths and angles characterize structure $\mathbf{2}^{+\bullet}$ as a genuine γ-distonic ion, rather than a loose ion/dipole complex ($\mathbf{3}^{+\bullet}$) of the ionized acetamide enol with neutral propene. For example, the C(2)/C(3) and C(3)/C(4) bonds in $\mathbf{2}^{+\bullet}$ (1.540 and 1.506 Å) almost match those in $\mathbf{1_1}^{+\bullet}$ (1.530 and 1.555 Å). While there exist numerous

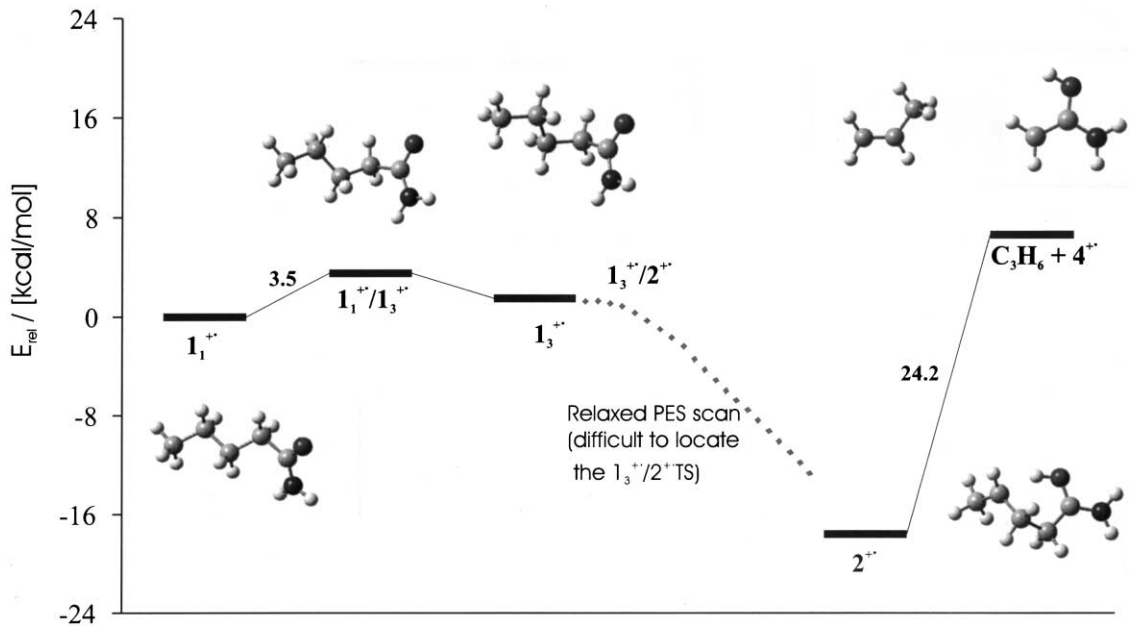

Fig. 3. Potential-energy surface for the loss of C_3H_6 from ionized valeramide (C_3-route) according to B3LYP6-311++G**//B3LYP6-31G* calculations.

indications for the existence of ion/dipole complexes in the chemistry of organic cation radicals [26], all our extensive attempts failed so far to locate a genuine minimum for $\mathbf{3}^{+\bullet}$, but instead always converged to $\mathbf{2}^{+\bullet}$. While this result should by no means dispute the possible existence of $\mathbf{3}^{+\bullet}$, it is entirely sufficient for the present purpose to state that structure $\mathbf{2}^{+\bullet}$ obviously is more stable than $\mathbf{3}^{+\bullet}$. Dissociation of $\mathbf{2}^{+\bullet}$ to the final products $\mathbf{4}^{+\bullet} + C_3H_6$ requires 24.2 kcal/mol at the B3LYP/6-311++G**//B3LYP/6-31G* level of theory, corresponding to an overall endothermicity of 6.6 kcal/mol for the reaction $\mathbf{1_1}^{+\bullet} \rightarrow \mathbf{4}^{+\bullet} + C_3H_6$ at 0 K. A more detailed consideration of the exit channels is postponed to a separate section further below.

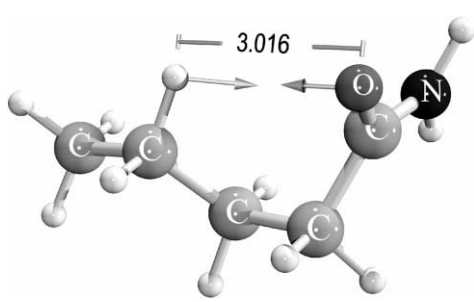

Fig. 4. Illustration of the movements of the hydrogen at C(4) and the carbonyl oxygen in the low-lying 89 cm^{-1} mode of conformer $\mathbf{1_3}^{+\bullet}$.

3.4.2. δ-C–H bond activation (C_2-route)

While a single C–C bond rotation is sufficient to achieve a reactive conformation for the McLafferty rearrangement, two rotations $\mathbf{1_1}^{+\bullet} \rightarrow \mathbf{1_2}^{+\bullet} \rightarrow \mathbf{1_4}^{+\bullet}$ (Fig. 5) are required for δ-C–H bond activation which initiates the C_2-route. Similar to the McLafferty rearrangement, the barrier associated with hydrogen migration is rather low, and the transition structure (TS) $\mathbf{1_4}^{+\bullet}/\mathbf{5_1}^{+\bullet}$ is only 1.2 kcal/mol above $\mathbf{1_4}^{+\bullet}$ (Fig. 6). Again, the barrier for C–C bond rotation exceeds that associated with hydrogen migration, but the difference is considerably smaller for activation of the δ-C–H bonds, consistent with the small, but non-negligible KIEs found upon deuteration at C(5) in the experimental studies. Similar to the C_3-route, the δ-distonic ion

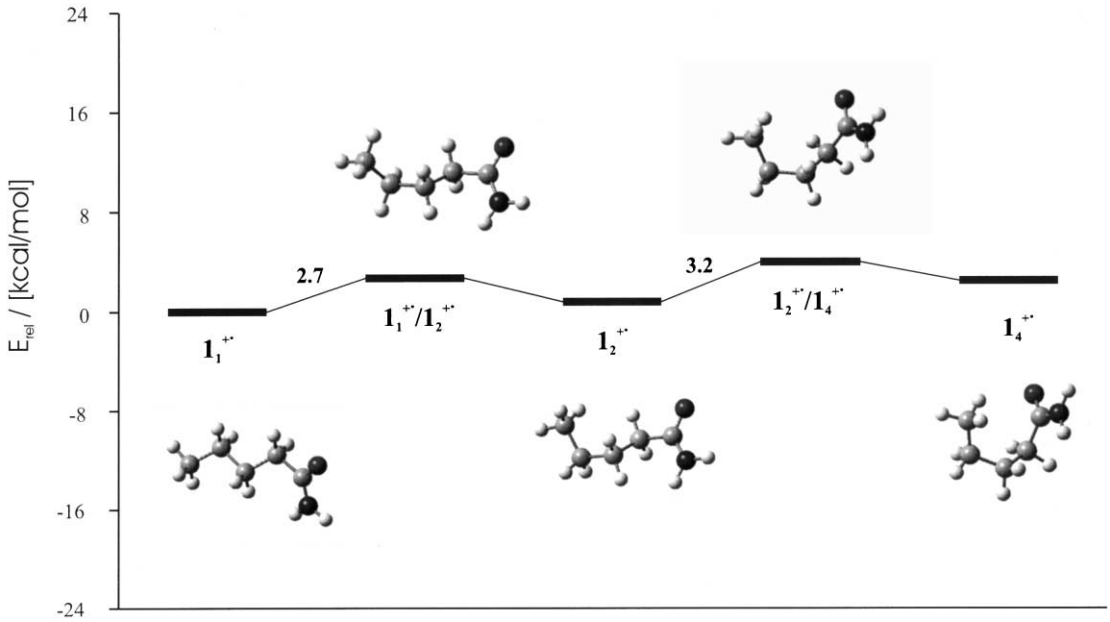

Fig. 5. Conformational changes of $\mathbf{1}^{+\bullet}$ required as a prerequisite for the access to the C_2-route according to B3LYP6-311++G**//B3LYP6-31G* calculations.

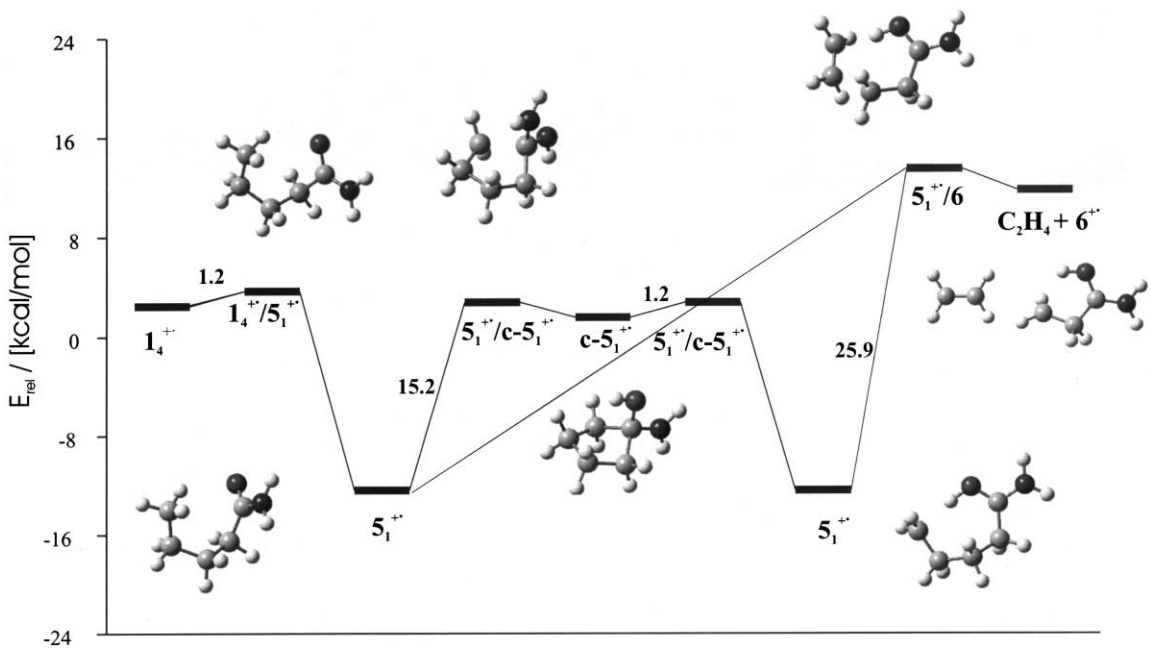

Fig. 6. Potential-energy surface for the loss of C_2H_4 from ionized valeramide (C_2-route) according to B3LYP6-311++G**//B3LYP6-31G* calculations.

$\mathbf{5_1}^{+\bullet}$ is 12.4 kcal/mol more stable than $\mathbf{1_1}^{+\bullet}$. Interestingly, structure $\mathbf{5_1}^{+\bullet}$ appears quite congested rather than exhibiting a more space-filling conformation. In order to investigate, whether or not this effect is due to an interaction between the charge and the spin centers in $\mathbf{5_1}^{+\bullet}$, other conformers were considered as well, including the seemingly ideal *all-anti*-orientation of the C–C bonds. In the resulting *all-anti*-conformer $\mathbf{5_4}^{+\bullet}$, the O–C(5) distance amounts to 6.225 Å compared to only 2.807 Å in $\mathbf{5_1}^{+\bullet}$. Though less strained, conformer $\mathbf{5_4}^{+\bullet}$ is ca. 8 kcal/mol less stable than $\mathbf{5_1}^{+\bullet}$. As a sum of strain and energy difference, we may therefore, roughly estimate that the interaction of the charge and spin centers leads to an additional stabilization in the order of 10 kcal/mol. A value of this magnitude is best rationalized by involving hydrogen bonding between the radical center and the hydroxy group, as also implied by the almost linear arrangement of the atoms involved ($\alpha_{C(5)HO} = 171.8^\circ$) together with $r_{C(5)H} = 1.806$ Å. In comparison, hydrogen bonding involving the amino group is energetically disfavored (conformer $\mathbf{5_2}^{+\bullet}$).

Any conformer of $\mathbf{5}^{+\bullet}$ could undergo C(3)–C(4) bond cleavage to afford the cation radical $\mathbf{6}^{+\bullet}$ concomitant with neutral ethene. At the B3LYP/6-311++G**//B3LYP/6-31G* level of theory, an overall endothermicity of 11.8 kcal/mol is predicted for the reaction $\mathbf{1_1}^{+\bullet} \rightarrow \mathbf{6}^{+\bullet} + C_2H_4$ at 0 K. Similar to the δ-distonic ion $\mathbf{5_1}^{+\bullet}$, the β-distonic ion $\mathbf{6}^{+\bullet}$ seems to experience stabilization by intramolecular hydrogen bonding because in the most stable conformer found the hydroxy group is oriented towards the radical site at C(3) with $r_{C(3)O} = 2.812$ Å and $\alpha_{C(3)HO} = 113.6^\circ$; however, $r_{C(3)H(O)} = 2.269$ Å indicates that hydrogen bonding is less efficient than in $\mathbf{5_1}^{+\bullet}$. A conformer in which the OH group points away from the backbone ($r_{C(3)O} = 3.019$ Å) is 4.3 kcal/mol less stable than $\mathbf{6}^{+\bullet}$ at the B3LYP/6-311++G**//B3LYP/6-31G* level of theory.

In competition with dissociation, $\mathbf{5_1}^{+\bullet}$ can isomerize to the cyclic structure c-$\mathbf{5}^{+\bullet}$ where the associated TS $\mathbf{5_1}^{+\bullet}$/c-$\mathbf{5_1}^{+\bullet}$ is energetically close to c-$\mathbf{5_1}^{+\bullet}$ (Table 3). The relatively low energy demand of this degenerate rearrangement is in perfect agreement with the pair-wise equilibration of the C(2)/C(3) and C(4)/C(5) positions as inferred from the experimental studies [1].

For the isomerization of the δ-distonic ion $\mathbf{5}^{+\bullet}$ to the ionized enol $\mathbf{7}^{+\bullet}$ via 1,4-hydrogen migration (Fig. 7), a conformational change is required first. Thus, the most stable conformer $\mathbf{5_1}^{+\bullet}$ must trade-off hydrogen bonding, giving rise to a conformer $\mathbf{5_3}^{+\bullet}$ in which one of the hydrogens at C(2) can interact with the radical site at C(5). While the barrier associated with hydrogen migration via TS $\mathbf{5_3}^{+\bullet}/\mathbf{7_1}^{+\bullet}$ is not very large (10.3 kcal/mol relative to $\mathbf{5_3}^{+\bullet}$), the resulting energy demand in conjunction with the required conformational changes locate TS $\mathbf{5_3}^{+\bullet}/\mathbf{7_1}^{+\bullet}$ at a relative energy of 4.8 kcal/mol above $\mathbf{1_1}^{+\bullet}$. Conformer $\mathbf{7_1}^{+\bullet}$ is 18.5 kcal/mol more stable than $\mathbf{1_1}^{+\bullet}$; conformer $\mathbf{7_2}^{+\bullet}$ and the associated TS $\mathbf{5_2}^{+\bullet}/\mathbf{7_2}^{+\bullet}$ are close in energy and primarily differ in the orientation of the functional group relative to the backbone. Any conformer of $\mathbf{7}^{+\bullet}$ could undergo C(3)–C(4) bond scission to yield $\mathbf{8}^{+} + C_2H_5^{\bullet}$, which requires 27.8 kcal/mol for conformer $\mathbf{7_1}^{+\bullet}$, corresponding to an overall endothermicity of 9.3 kcal/mol relative to $\mathbf{1_1}^{+\bullet}$ at the B3LYP/6-311++G**//B3LYP/6-31G* level of theory at 0 K.

3.4.3. β-C–H bond activation (C_1-route)

1,4-Hydrogen transfer can directly proceed from conformer $\mathbf{1_1}^{+\bullet}$, and the associated TS $\mathbf{1_1}^{+\bullet}/\mathbf{1_1}^{+\bullet}$ requires only 1.9 kcal/mol (Fig. 8). The facile hydrogen migration can be attributed to the fact that the resulting β-distonic ion $\mathbf{1_1}^{+\bullet}$ is 13.2 more stable than $\mathbf{1_1}^{+\bullet}$. Once more, the distonic ion formed seems to experience stabilization via hydrogen bonding, because in the computed minimum, the hydroxy group points towards the radical site with $r_{C(3)H(O)} = 2.190$ Å, $r_{C(3)O} = 2.190$ Å, and $\alpha_{C(3)HO} = 116.4^\circ$. Interestingly, the subsequent C(4)–C(5) bond cleavage of $\mathbf{1_1}^{+\bullet}$ is associated with a significant barrier in the exit channel, TS $\mathbf{1_1}^{+\bullet}/\mathbf{12}^{+}$. For the final products $\mathbf{12}^{+} + CH_3^{\bullet}$, an endothermicity of 8.4 kcal/mol relative to $\mathbf{1_1}^{+\bullet}$ is predicted at the B3LYP/6-311++G**//B3LYP/6-31G* level of theory at 0 K.

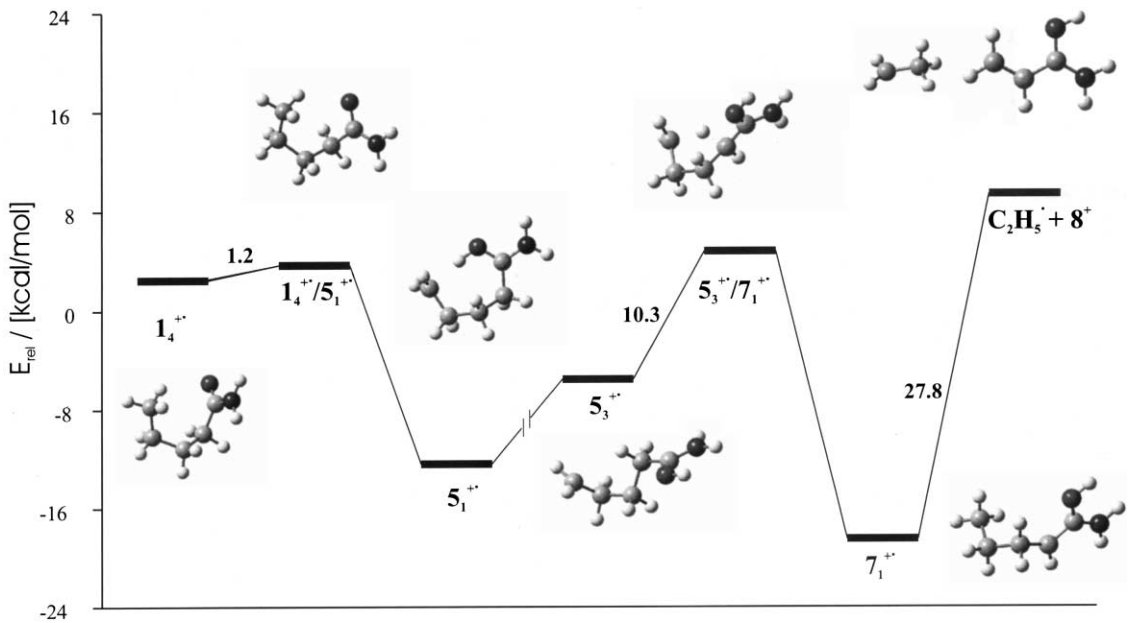

Fig. 7. Potential-energy surface for the indirect loss of $C_2H_5^{\bullet}$ from ionized valeramide (C_2-route) according to B3LYP6-311++G**//B3LYP6-31G* calculations.

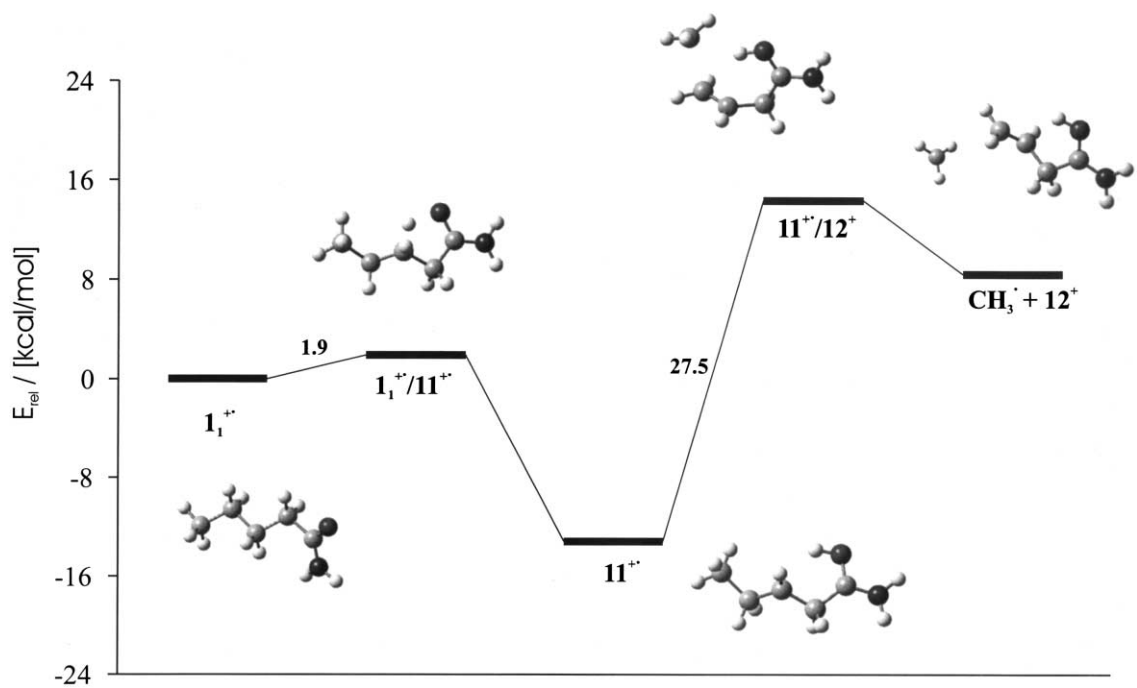

Fig. 8. Potential-energy surface for the loss of $CH_3^{\bullet}$ from ionized valeramide (C_1-route) according to B3LYP6-311++G**//B3LYP6-31G* calculations.

3.4.4. α-C–H bond activation (keto/enol tautomerism)

Even though the *all-anti*-conformer of the ionized enol $\mathbf{7_3}^{+\bullet}$ ($E_{rel} = -20.3$ kcal/mol) is most likely the global minimum of all cationic species examined here, the computed energy demand of 23.2 kcal/mol associated with intramolecular keto/enol tautomerism via 1,3-hydrogen transfer via TS $\mathbf{1_1}^{+\bullet}/\mathbf{7_3}^{+\bullet}$ is much higher than those of all other hydrogen migrations. This result is not at all unexpected, since previous studies have amply demonstrated that the facile keto/enol tautomerism known from the condensed phase occurs intermolecularly, whereas intramolecular keto/enol tautomerism via 1,3-hydrogen migration is associated with considerable barriers for neutral as well as cationic carbonyl compounds [27]. In the present case, formation of the ionized enol is indeed more likely to occur via the much more complicated, multi-step sequence $\mathbf{1_1}^{+\bullet} \rightarrow \mathbf{1_2}^{+\bullet} \rightarrow \mathbf{1_4}^{+\bullet} \rightarrow \mathbf{5_1}^{+\bullet} \rightarrow \mathbf{7_1}^{+\bullet} \rightarrow \mathbf{7_3}^{+\bullet}$ described in the context of the C_2-route. Accordingly, we conclude that direct keto/enol tautomerism will not contribute to the dissociation behavior of ionized valeramide. The ionized enol might be involved, however, if some neutral **7** were present in the precursor, because ionization of the enol is much easier than that of the keto, $IE_a(\mathbf{7}) = 7.19$ eV with B3LYP/6-311++G**//B3LYP/6-31G*. However, at the same level of theory the neutral enol **7** is computed to be 24.9 kcal/mol less stable than neutral valeramide ($\mathbf{1_1}$), such that contributions from the enol form can be excluded rigorously at 298 K. Note that similar stability differences have been predicted for the keto/enol tautomers of neutral acetamide [28].

3.4.5. Exit channels

With respect to products formed upon dissociation of ionized valeramide, two general and one specific point need to be addressed.

The first general concern is the choice of the basis sets in the computational study. Upon inspection of the data compiled in Table 4, it becomes immediately obvious that the dissociation enthalpies relative to $\mathbf{1_1}^{+\bullet}$ show a pronounced basis set effect. The general tendency for decreasing endothermicities with the larger basis set can be attributed to a basis set superposition error. The deviations of ΔE_{rel} are, however, not at all uniform and most likely seem to reflect the role of electron correlation in the various fragments. For example, ΔE_{rel} is small for the saturated, cyclic species $\mathbf{10}^+$ and $\mathbf{13}^+$ and large for unsaturated fragments such as $\mathbf{4}^{+\bullet}$, $\mathbf{6}^{+\bullet}$, $\mathbf{8}^+$, and $\mathbf{12}^+$. Irrespective of the precise origin of these effects, these trends indicate that even the larger basis set used might not suffice to describe the exit channels within a few kcal/mol. This has to be kept in mind as a note of caution for the entire PES of ionized valeramide, even though the computed data compare quite favorably with the experimental data available. Nevertheless, we note in passing that the use of B3LYP/6-31G* geometries appears adequate, because exploratory geometry optimizations of $\mathbf{1}^{+\bullet}$, $\mathbf{4}^{+\bullet}$, and $\mathbf{5_1}^{+\bullet}$ at the B3LYP/6-311++G** level of theory led to differences of maximal 0.01 Å in bond lengths and maximal 0.1 kcal/mol in the relative energetics.

The second general aspect concerns thermal contributions. In the mass spectrometric experiments described in [1], the valeramide samples were evaporated at room temperature. Therefore, the relative energies computed for 0 and 298 K are compared with each other, where the difference $\Delta E_{thermal}$ represents a measure for the importance of thermal contributions (Table 5). While thermal effects hardly change the energetics associated with the intramolecular rearrangements of ionized valeramide, all exit channels are lowered by about 10 kcal/mol relative to $\mathbf{1_1}^{+\bullet}$, simply because of entropy as two particles are formed out of one. Hence, the slightly endothermic expulsion of propene via the McLafferty route ($E_0 = 6.6$ kcal/mol at 0 K) becomes exoergic at room temperature ($E_0 = -4.1$ kcal/mol). Thermal contributions can thereby explain the observation of the enol fragment $\mathbf{4}^{+\bullet}$ due to the McLafferty rearrangement right at the onset of photoionization as described in [1]. Moreover, while at 0 K the indirect loss of $C_2H_5^\bullet$ as well as the McLafferty reaction are subject to thermodynamic control due to the exit channels, both switch to kinetic control by the intermediate barriers at 298 K due to the entropic gains of the associated exit channels.

Table 4
Electronic energies (E_{tot}, in Hartree), zero-point energies (ZPE, in Hartree), and relative energies (E_{rel}, in kcal/mol)[a] of the dissociation products of ionized valeramide

	B3LYP/6-31G*//B3LYP/6-31G*			B3LYP/6-311++G**//B3LYP/6-31G*		
	E_{tot}	ZPE	E_{rel}[b]	E_{tot}	E_{rel}[b,c]	ΔE_{rel}[d]
4$^{+\bullet}$	−208.892507	0.073921		−208.962891[e]		
C_3H_6	−117.907562	0.080097		−117.945597[e]		
4$^{+\bullet}$ + C_3H_6	−326.800069	0.154018	14.6	−326.908488	6.6	8.0
6$^{+\bullet}$	−248.203109	0.101795		−248.283773		
C_2H_4	−78.587457	0.051208		−78.615509		
6$^{+\bullet}$ + C_2H_4	−326.790566	0.153003	19.9	−326.899282	11.8	8.1
8^{+}	−247.637169	0.092884		−247.717762		
$C_2H_5^{\bullet}$	−79.157868	0.059651		−79.185027		
8^{+} + $C_2H_5^{\bullet}$	−326.795037	0.152535	16.8	−326.902789	9.3	7.5
9^{+}	−247.630846	0.094573		−247.702183		
9^{+} + $C_2H_5^{\bullet}$	−326.788714	0.154224	21.8	−326.887210	20.1	1.7
10^{+}	−247.517747	0.087524		−247.591683		
10^{+} + $C_2H_5^{\bullet}$	−326.675615	0.147175	88.3	−326.776710	84.9	3.4
13^{+}	−247.617520	0.093827		−247.689936		
13^{+} + $C_2H_5^{\bullet}$	−326.775388	0.153478	29.7	−326.874963	27.3	2.4
14^{+}[f]	−247.577271	0.088982		−247.655572		
14^{+} + $C_2H_5^{\bullet}$	−326.735139	0.148633	52.0	−326.840599	45.9	6.1
12^{+}	−286.956919	0.121632		−287.048005		
$CH_3^{\bullet}$	−39.838292	0.029832		−39.855179		
12^{+} + $CH_3^{\bullet}$	−326.795211	0.151464	16.1	−326.903184	8.4	7.7

[a] Relative energies can only be given for the sums of fragments having the same composition as valeramide, where the lowest-lying conformer $\mathbf{1_1}^{+\bullet}$ of the cation radical is used as the reference point. This structure is best described as a complex of a $OCNH_2^+$ cation with ethene.

[b] ZPEs included with a scaling factor of 0.9805.

[c] ZPEs taken from the B3LYP/6-31G* calculations.

[d] Defined as $\Delta E_{rel} = E_{rel}$(B3LYP/6-31G*) − E_{rel}(B3LYP/6-311++G**).

[e] Energies at B3LYP/6-311++G**//B3LYP/6-311++G**: $\mathbf{4}^{+\bullet}$, −208.9629654, C_3H_6, −117.9456353.

[f] This structure corresponds to *N*-protonated β-propiolactame.

The specific aspect is the nature of the ionic fragment generated in the direct loss of $C_2H_5^{\bullet}$. The indirect route leads to protonated acrylamide $\mathbf{8}^{+}$, which appears to be the global minimum of the $[C_3,H_5,N,O]^+$ surface [29]. At the B3LYP/6-311++G**//B3LYP/6-31G* level of theory, the corresponding exit channel $\mathbf{8}^{+}$ + $C_2H_5^{\bullet}$ is situated at E_{rel} = 9.2 and −1.8 kcal/mol at 0 and 298 K, respectively, and the 0 K value is used as a reference for the other options for $C_2H_5^{\bullet}$ expulsions. Four different structures directly accessible from ionized valeramide were studied theoretically. The energetically most stable of these direct products is the protonated aminooxetane $\mathbf{9}^{+}$, which requires that C–C bond cleavage is assisted by simultaneous C–O bond formation. Formation of $\mathbf{9}^{+}$ is energetically more demanding than that of $\mathbf{8}^{+}$ by 10.8 kcal/mol. In contrast, direct C–C bond cleavage without formation of a new bond leads to the high-energy isomer $\mathbf{10}^{+}$ located 75.8 kcal/mol above $\mathbf{8}^{+}$. Alternatively to assisting C–O bond formation, C–N bond formation might lead to $\mathbf{13}^{+}$, i.e., *N*-protonated propiolactane (also known as 2-acetidinone). Isomer $\mathbf{13}^{+}$ is, however, 7.2 kcal/mol less stable than $\mathbf{9}^{+}$ and 18.0 kcal/mol disfavored against $\mathbf{8}^{+}$. Finally, the computational search also revealed a minimum $\mathbf{14}^{+}$ which is best described as a complex of a $OCNH_2^+$ cation with neutral ethene.

Table 5
Relative energies (E_{rel} in kcal/mol with $\mathbf{1_1}^{+\bullet}$ as the reference) of several points of the potential-energy surface of ionized valeramide and some of the relevant dissociation channels at 0 and 298 K, respectively, and the resulting thermal contributions ($\Delta E_{thermal}$ in kcal/mol) derived from the B3LYP/6-311++G**//B3LYP/6-31G* calculations[a]

	$E_{rel,0}$[b]	E_{298}[c]	$\Delta E_{thermal}$[d]
$\mathbf{1_1}^{+\bullet}/\mathbf{1_3}^{+\bullet}$	3.4	4.0	0.6
$\mathbf{2_1}^{+\bullet}$	−17.6	−16.6	1.0
$\mathbf{4}^{+\bullet} + C_3H_6$	6.6	−4.1	−10.7
$\mathbf{5_1}^{+\bullet}$	−12.5	−11.2	1.3
$\mathbf{5_1}^{+\bullet}/\mathbf{6}^{+\bullet}$	13.5	14.3	0.8
$\mathbf{5_3}^{+\bullet}/\mathbf{7_1}^{+\bullet}$	4.7	6.2	1.5
$\mathbf{6}^{+\bullet} + C_2H_4$	11.7	1.8	−9.9
$\mathbf{7_3}^{+\bullet}$	−20.3	−20.1	0.2
$\mathbf{8}^{+} + C_2H_5^{\bullet}$	9.2	−1.8	−11.0
$\mathbf{9}^{+} + C_2H_5^{\bullet}$	20.0	9.6	−10.4
$\mathbf{1_1}^{+\bullet}$	−13.2	−13.1	0.1
$\mathbf{1_1}^{+\bullet}/\mathbf{12}^{+}$	14.3	14.6	0.3
$\mathbf{12}^{+} + C_2H_5^{\bullet}$	8.3	−0.3	−8.6

[a] Unscaled frequencies used.
[b] Relative energy at 0 K.
[c] Relative energy at 298 K including enthalpic and entropic effects.
[d] Defined as $\Delta E_{thermal} = E_{298} - E_0$.

3.5. Comparison with literature thermochemistry

Using thermochemical databases [30] in combination with selected isodesmic reactions,[2] the heat of formation of gaseous valeramide can be estimated as $\Delta_f H^\circ(1) = -71.3 \pm 0.9$ kcal/mol. Combination with IE(1) = 9.40 ± 0.03 eV derived from the photoionization experiments [1] leads to $\Delta_f H^\circ(\mathbf{1}^{+\bullet}) = 145.5 \pm 1.4$ kcal/mol. Next, the heat of formation of acetamide (−57.0 ± 0.2 kcal/mol) combined with its IE (9.69 ± 0.07 eV) and the stability difference of 18.9 kcal/mol in favor of the ionized enol predicted by G2 calculations [31] suggest $\Delta_f H^\circ(\mathbf{4}^{+\bullet}) = 147.6 \pm 2.5$ kcal/mol.[3] In conjunction with $\Delta_f H^\circ(C_3H_6) = 4.9$ kcal/mol for propene, fragmentation of $\mathbf{1}^{+\bullet}$ via the C_3-route is therefore, predicted to be endothermic by 7.0 ± 2.9 kcal/mol. This figure compares nicely with the computed reaction enthalpy of 6.6 kcal/mol (Table 4). Likewise, the heat of formation of acrylamide,[4] its proton affinity [32] and the heat of formation of ethyl radical [33] predict an endothermicity of 10.0 ± 1.6 kcal/mol for the indirect loss of $C_2H_5^{\bullet}$ via the C_2-route which compares well with the computed figure of 9.3 kcal/mol. Literature values further suggest an endothermicity of about 10 kcal/mol[5] for the loss of $CH_3^{\bullet}$ via the C_1-route compared to a computed value of 8.4 kcal/mol for $\mathbf{12}^{+} + CH_3^{\bullet}$. Finally, the relative energetics of the $[C_2,H_5,N,O]^{+}$ isomers $\mathbf{8}^{+}$, $\mathbf{9}^{+}$, and $\mathbf{13}^{+}$ are qualitatively consistent with earlier computations at the HF level [29].

4. Implications for the fragmentation behavior of ionized valeramide

Comparing the theoretical studies reported here with the results of the mass spectrometric experiments presented in [1] leads to a consistent description of the dissociation behavior of ionized valeramide. Thus, despite of the limitations of the computational approach used, the B3LYP/6-311++G**//B3LYP/6-31G* level of theory appears to describe the energetics of ionized valeramide and its rearrangement reasonably well. Moreover, the energetic order of the fragmentation channels is the same for both approaches: loss of propene is most facile and the indirect elimination of $C_2H_5^{\bullet}$ can occur at slightly higher energies, while losses of $CH_3^{\bullet}$ and C_2H_4 as well as the direct elimination of $C_2H_5^{\bullet}$ require elevated energies. For a quantitative comparison, let us consider the point of highest energy demand in each route. At room temperature, the C_3-route is subject to kinetic control via TS $\mathbf{1_1}^{+\bullet}/\mathbf{1_3}^{+\bullet}$ in that the access to this pathways is determined by conformational changes of the cation radical $\mathbf{1}^{+\bullet}$. This situation is consistent

[2] In the isodesmic reactions, processes such as $RCONH_2 + n\text{-}C_4H_9COOH \rightarrow RCOOH + n\text{-}C_4H_9CONH_2$ were assumed to be thermoneutral.
[3] An average error of ±2 kcal/mol is assigned to the G2 calculations and used in the error estimation.
[4] Taken from [30b]. Note that [30a] lists a misleading value.
[5] No error bar is given because the estimation of the unknown proton affinity of vinylacetamide is ambiguous. Here, PA(vinylacetamide) = PA(acrylamide) = 208 kcal/mol was used.

with the negligible kinetic isotope effect upon deuteration of the C(4) position derived from experiment (KIE(γ-CH) = 1.01). In contrast, the indirect loss of $C_2H_5^\bullet$ via the C_2-route is controlled by three barriers of similar energy demands relative to $\mathbf{1_1}^{+\bullet}$ as the reference: TS $\mathbf{1_2}^{+\bullet}/\mathbf{1_4}^{+\bullet}$ (E_{rel} = 4.0 kcal/mol), TS $\mathbf{1_4}^{+\bullet}/\mathbf{5_1}^{+\bullet}$ (E_{rel} = 3.7 kcal/mol), and TS $\mathbf{5_3}^{+\bullet}/\mathbf{7_1}^{+\bullet}$ (E_{rel} = 4.8 kcal/mol) of which the first is a conformational barrier while the two latter are associated with hydrogen migrations. Involvement of all three TSs in the overall reaction is consistent with the more pronounced KIEs in this route for both, the C(2) and the C(5) positions as derived from the kinetic modeling (KIE(δ-CH) = 1.3 and KIE(H/D, C_2) = 1.8). The slightly larger barriers of this route compared to the McLafferty rearrangement and the lower overall exoergicity of the C_2-route also agree favorably with the strong preference of the C_3-route in the photoionization studies and the difference of 0.15 ± 0.07 eV (3.5 kcal/mol) of the associated appearance energies. According to the calculated energy profiles, loss of C_2H_4 is thermodynamically controlled by the height of the exit channel which lies ca. 6 kcal/mol above the energy demand for loss of propene. With regard to the expected occurrence of a kinetic shift due to the competing C_3-route as well as the uncertainties of the computational approach, this figure is qualitatively consistent with a difference of 0.7 ± 0.1 eV (16 kcal/mol) of the associated appearance energies. The computations predict loss of $CH_3^\bullet$ (C_1-route) to be subject to kinetic control due to TS $\mathbf{1_1}^{+\bullet}/\mathbf{12}^+$ (E_{rel} = 14.3 kcal/mol) operative in the exit channel. This energy demand is much larger than those of the competing channels which is in agreement with the low abundance of $CH_3^\bullet$ elimination in the various kinds of mass spectrometric experiments. Nevertheless, the appearance of the $[M–CH_3^\bullet]^+$ fragment about 1.5 ± 0.2 eV (35 kcal/mol) above the photoionization threshold of valeramide indicates the operation of a substantial kinetic shift in this minor channel and/or an underestimation of the barrier in the computations. Finally, the theoretical data shed some light on the structure of the fragment ion formed via the direct loss of $C_2H_5^\bullet$. Experimentally, the direct route becomes apparent at about 1 eV above photoionization threshold. This amount of excess energy is clearly insufficient for the formation of $\mathbf{10}^+$ as well as $\mathbf{14}^+$ in the direct route, and it is therefore, concluded that C–C bond cleavage is accompanied by C–O and/or C–N bond formation to yield $\mathbf{9}^+$ and/or $\mathbf{13}^+$, respectively.

As far as H/D equilibration in the dissociation of ionized valeramide is concerned, the following conclusions emerge from the theoretical study. At first, the pair-wise equilibration of the C(2)/C(3) and C(4)/C(5) positions in the indirect loss of $C_2H_5^\bullet$ as inferred from experiment is supported by the location of the degenerate TS $\mathbf{5_1}^{+\bullet}$/c-$\mathbf{5}^+$ below TS $\mathbf{5_3}^{+\bullet}/\mathbf{7_1}^+$ associated with 1,4-hydrogen transfer from C(2) to the radical center at C(5). Moreover, the fact that TS $\mathbf{1_4}^{+\bullet}/\mathbf{5_1}^+$ is less demanding than TS $\mathbf{5_3}^{+\bullet}/\mathbf{7_1}^+$, in particular with respect to the preceding minima, lends support to the significantly larger KIE associated with the latter, as derived from the kinetic modeling of the experimental isotope distributions obtained in the metastable ion studies. While we have not theoretically addressed H/D exchange in the McLafferty route, the uncoupling of the C_2- and C_3-routes deduced from the experiments is also supported by the results of the calculations in that the population of these two routes is primarily determined by the accessibility of the adequate conformers. In fact, with regard to the relative stabilities of the distonic ions $\mathbf{2}^{+\bullet}$ and $\mathbf{5}^{+\bullet}$, their mutual interconversion via the different conformers of $\mathbf{1}^{+\bullet}$ is considered unlikely, particularly in view of the competition by the low-lying fragmentation channels.

While all these results agree pretty well, the theoretical results provide no indication, not even a hint, for the variations in the C_3/C_2 branching observed in various experiments. Thus, irrespective of basis set, temperature etc., the C_3-route is always clearly preferred over the C_2-route. Accordingly, at least the static picture of the calculated PES of ionized valeramide in terms of minima and transition structures does not provide a rationale for the ca. 1:1 ratio of the C_2- and C_3-channels observed in the metastable ion studies conducted in the sector experiment.

5. Conclusions

The theoretical study of ionized valeramide using B3LYP leads to the construction of a potential-energy surface for the dissociation behavior of the cation radical which is fairly consistent with the results of the mass spectrometric studies presented the preceding article. Thus, the calculated PES agrees with respect to the energetic ordering of the fragmentation channels observed and confirms the mechanistic schemes derived from analysis of the labeling data. In fact, even subtle details of the proposed fragmentation schemes, e.g., the pair-wise equilibration of C(2)/C3(3) with C(4)/C3(5), as well as kinetic isotope effects are qualtitatively confirmed by theory. As far as competition between the fragmentation different channels is concerned, the computed results agree qualitatively with the branching ratios obtained in the photoionization studies. Thus, the McLafferty rearrangement (C_3-route) has the lowest energy demand, while the computed pathways for losses of $CH_3^{\bullet}$, C_2H_4, and $C_2H_5^{\bullet}$, respectively, are somewhat higher in energy, but of comparable magnitude. Quite remarkable is the effect of thermal contributions on the dissociation behavior, in that at 0 K all fragmentations are thermochemically controlled by the height of the exit channels, whereas kinetic control due to intermediate barriers is most important at 298 K or higher temperatures. The missing link between experiment and theory concerns the unusual variations in the C_3/C_2 ratios observed in some of the experiments. While the theoretical results support the idea that the experimentally observed routes are uncoupled from each other, i.e., the H-migrations from various positions occur quasi-irreversibly, none of the computed properties can explain, why a C_3/C_2 ratio of about 1 is observed for metastable $\mathbf{1}^{+\bullet}$ in the sector-field instrument.

In a more general sense, the computational exploration of the potential-energy surface of the molecular ion of valeramide suggests that various kinds of C–H bond activations are possible for ionized carbonyl compounds. Instead of a kinetic control by the barrier associated with hydrogen migration, the regioselectivity of C–H bond activation seems to be determined by the accessibility of the appropriate conformations in the parent ion as well as the energetics of the associated exit channels. In fact, the present results suggest that the prevalence of the McLafferty rearrangement in the mass spectrometric fragmentation of carbonyl compounds is not primarily due to a particular preference of 1,5-hydrogen transfer, but results from the favorable energy demand of the dissociation products.

Acknowledgements

Financial support by the Deutsche Forschungsgemeinschaft, the Fonds der Chemischen Industrie, the Volkswagen-Stiftung, and the Gesellschaft von Freunden der Technischen Universität Berlin is gratefully acknowledged. We are particularly indebted to the Konrad-Zuse Zentrum for the generous allocation of computer time. M.S. also thanks the Ernst Schering Research Foundation for a research fellowship. Finally, we thank Dipl.-Chem. M. Diefenbach for assistance in the preparation of Fig. 4.

Appendix A. Cartesian coordinates of the stationary points

$\mathbf{1_1}$				$\mathbf{1_2}$			
C	−2.192153	0.056907	0.091421	C	2.114114	−0.534951	0.124909
C	−0.708766	0.442367	0.055332	C	0.783562	0.208765	−0.056177
C	−3.123306	1.273545	0.104409	C	3.337574	0.337627	−0.171315
C	0.227113	−0.770671	0.042353	C	−0.433485	−0.674586	0.253841

(*contd on next page*)

Appendix A (continued)

C	1.692844	−0.374795	−0.135773	C	−1.821306	−0.088212	−0.010619
N	2.597030	−1.205086	0.473704	N	−1.946998	1.269359	0.131652
O	2.043775	0.605955	−0.775554	O	−2.779070	−0.799056	−0.278143
H	−2.390273	−0.564606	0.976745	H	2.123525	−1.416699	−0.530519
H	−2.425101	−0.572716	−0.779576	H	2.175564	−0.918861	1.152810
H	−0.470297	1.073022	0.922854	H	0.717130	0.584727	−1.087006
H	−0.495075	1.052038	−0.829732	H	0.789779	1.092481	0.600302
H	−4.176573	0.971265	0.123411	H	4.268499	−0.224639	−0.038305
H	−2.970003	1.897218	−0.784540	H	3.376969	1.207867	0.495615
H	−2.940696	1.902659	0.984192	H	3.318808	0.711043	−1.202550
H	−0.035253	−1.429008	−0.799516	H	−0.410711	−0.977318	1.310694
H	0.099940	−1.370111	0.953908	H	−0.391379	−1.601428	−0.327559
H	3.577652	−1.056717	0.279006	H	−2.841077	1.676304	−0.105728
H	2.321883	−2.079209	0.895292	H	−1.148314	1.881598	0.191992
$1_1^{+\bullet}$				**$1_2^{+\bullet}$**			
C	−2.148100	0.259261	0.030934	C	−2.081099	−0.890429	0.025456
C	−0.616561	0.501806	0.141982	C	−0.556795	−0.834701	0.331188
C	−2.910371	1.482329	0.564603	C	−2.895283	0.279735	0.566600
C	0.107611	−0.763611	−0.350929	C	0.080090	0.308949	−0.481360
C	1.652479	−0.626389	−0.252139	C	1.602946	0.418248	−0.226056
N	2.259197	−0.150884	0.813116	N	2.417186	−0.612228	−0.281146
O	2.228057	−1.044823	−1.276394	O	1.951119	1.594809	0.007760
H	−2.422812	−0.635946	0.600497	H	−2.414760	−1.827293	0.498595
H	−2.407808	0.073952	−1.017102	H	−2.239478	−1.015765	−1.052429
H	−0.359206	0.722668	1.184857	H	−0.096341	−1.793454	0.066525
H	−0.337578	1.369217	−0.464874	H	−0.406359	−0.673723	1.404068
H	−3.986459	1.288401	0.471992	H	−3.962647	0.096712	0.399362
H	−2.676583	2.385652	−0.007168	H	−2.663521	1.227262	0.064463
H	−2.693834	1.669969	1.621227	H	−2.745340	0.413335	1.643376
H	−0.140969	−0.978921	−1.393115	H	−0.372768	1.270556	−0.225967
H	−0.125835	−1.660394	0.240088	H	−0.010420	0.178672	−1.569459
H	3.273339	−0.104265	0.859528	H	3.416247	−0.498809	−0.133072
H	1.728564	0.164060	1.616701	H	2.066979	−1.541183	−0.484490
$1_3^{+\bullet}$				**$1_4^{+\bullet}$**			
C	−1.562524	−0.050752	0.598999	C	0.296024	−2.155933	−0.051881
C	−0.824784	−0.545535	−0.651818	C	−1.119887	−1.660363	0.280571
C	−2.685965	−0.997176	1.036189	O	1.440341	1.166342	1.031913
C	0.253392	0.408654	−1.195033	C	0.686134	1.119106	0.033851
C	1.449710	0.496581	−0.218629	C	−0.798208	0.934258	0.430651
N	2.281458	−0.503111	−0.031933	C	−1.466699	−0.271959	−0.263866

(*contd on next page*)

Appendix A (continued)

O	1.520423	1.602967	0.363967	N	1.078357	1.253351	−1.212368
H	−1.970415	0.948996	0.403496	H	0.421479	−3.185056	0.296671
H	−0.842046	0.057776	1.424658	H	0.483920	−2.149843	−1.131896
H	−1.543249	−0.628077	−1.484618	H	1.071957	−1.557435	0.441627
H	−0.409915	−1.548253	−0.492957	H	−1.285068	−1.674866	1.365281
H	−3.177614	−0.614906	1.935103	H	−1.845618	−2.365221	−0.144440
H	−2.301604	−1.997535	1.264366	H	−1.255962	1.898208	0.163644
H	−3.448284	−1.094319	0.255515	H	−0.852700	0.835929	1.518864
H	−0.150287	1.415136	−1.336974	H	−2.538849	−0.079005	−0.087096
H	0.700884	0.088641	−2.147683	H	−1.320950	−0.227521	−1.350391
H	3.057200	−0.430838	0.621124	H	0.409032	1.212085	−1.972796
H	2.172761	−1.369204	−0.548484	H	2.057359	1.397883	−1.444145
$1_1^{+\bullet}/1_2^{+\bullet}$				**$1_1^{+\bullet}/1_3^{+\bullet}$**			
C	−2.112357	−0.632760	−0.056655	C	−1.942874	0.083247	0.493050
C	−0.610652	−0.539868	0.398384	C	−0.770782	−0.495048	−0.304286
C	−3.063927	0.023753	0.942883	C	−2.930043	−1.010003	0.925603
C	0.161843	0.236873	−0.680978	C	0.201992	0.603913	−0.833889
C	1.677880	0.355567	−0.339661	C	1.622531	0.431064	−0.258460
N	2.403623	−0.678917	0.025610	N	2.348130	−0.646970	−0.453567
O	2.104374	1.516934	−0.482307	O	1.994584	1.435127	0.391085
H	−2.339960	−1.698757	−0.184049	H	−2.457210	0.836258	−0.117371
H	−2.251559	−0.181606	−1.047317	H	−1.560625	0.605037	1.381212
H	−0.190359	−1.541640	0.534474	H	−1.129422	−1.030404	−1.197431
H	−0.543100	−0.020875	1.359189	H	−0.250007	−1.247471	0.301169
H	−4.096896	−0.087665	0.592255	H	−3.756497	−0.563099	1.486722
H	−2.871330	1.097897	1.049179	H	−2.450170	−1.753307	1.571793
H	−2.983946	−0.438234	1.932107	H	−3.354800	−1.530615	0.060560
H	−0.233186	1.249200	−0.793759	H	−0.152157	1.604466	−0.570146
H	0.143785	−0.243275	−1.669617	H	0.354248	0.592965	−1.922685
H	3.397444	−0.578746	0.212755	H	3.287029	−0.727080	−0.072276
H	1.992033	−1.600740	0.110125	H	1.991083	−1.418011	−1.007366
$1_2^{+\bullet}/1_4^{+\bullet}$				**$2^{+\bullet}$**			
C	−2.068236	−0.771986	−0.053528	C	−1.510497	0.516386	0.598064
C	−0.603184	−1.162050	−0.262098	C	−1.144316	−0.713119	−0.190969
C	−2.287462	0.344097	0.974346	C	−2.530906	1.479113	0.090736
C	0.226147	−0.062622	−1.000087	C	0.248545	−1.288517	0.162289
C	1.396026	0.474112	−0.151597	C	1.360572	−0.318732	−0.122161
N	2.279834	−0.302824	0.432485	N	2.542410	−0.711644	−0.531185
O	1.415110	1.726156	−0.121392	O	1.197770	0.956223	0.046811
H	−2.591182	−1.677824	0.284547	H	0.238075	1.143777	0.311088

(*contd on next page*)

Appendix A (continued)

H	−2.514923	−0.500793	−1.018085	H	−1.374535	0.455339	1.681103
H	−0.524200	−2.057982	−0.896309	H	−1.205405	−0.512965	−1.267888
H	−0.156909	−1.431126	0.703154	H	−1.877075	−1.512571	0.008149
H	−3.354483	0.552351	1.091331	H	−2.507755	2.424386	0.641759
H	−1.809845	1.284180	0.667786	H	−3.545727	1.064451	0.224311
H	−1.892691	0.066077	1.958390	H	−2.414086	1.685591	−0.979207
H	−0.403750	0.785898	−1.283144	H	0.436448	−2.226948	−0.367899
H	0.716840	−0.414200	−1.918935	H	0.295862	−1.514863	1.238019
H	3.056742	0.086361	0.959941	H	3.285194	−0.034186	−0.685767
H	2.214943	−1.311731	0.352846	H	2.749595	−1.691071	−0.687602
$5_1^{+\bullet}$				**$5_2^{+\bullet}$**			
C	0.108989	−2.265565	0.443730	C	−1.071061	−1.299823	−0.856676
C	−1.219612	−1.606030	0.630702	C	0.268404	−1.529516	−0.130951
O	1.539186	0.086326	−0.107560	C	−2.210848	−0.876069	0.014184
C	0.686089	1.054957	−0.214798	C	0.701419	−0.407052	0.860821
C	−0.760349	0.931396	0.173301	C	0.772624	0.952635	0.246832
C	−1.487726	−0.369791	−0.257837	N	−0.316099	1.639005	−0.000891
N	1.168121	2.190581	−0.663466	O	1.968678	1.398662	−0.027565
H	0.593350	−2.763017	1.281076	H	−1.334733	−2.249012	−1.356254
H	0.387914	−2.620564	−0.549468	H	−0.944975	−0.588870	−1.685512
H	1.114705	−0.784909	0.202478	H	1.063580	−1.690419	−0.865861
H	−1.379140	−1.348524	1.684559	H	0.212776	−2.439545	0.475771
H	−1.995843	−2.352287	0.385080	H	−3.125591	−0.510143	−0.445747
H	−1.290893	1.799963	−0.228761	H	−2.303877	−1.264257	1.026674
H	−0.796251	1.028601	1.269039	H	1.688038	−0.635932	1.270192
H	−2.556687	−0.141693	−0.210363	H	−0.011003	−0.358755	1.690905
H	−1.269280	−0.594518	−1.308929	H	−0.321540	2.561759	−0.427383
H	0.581527	3.007982	−0.780274	H	−1.221422	1.190532	0.185888
H	2.155910	2.274492	−0.890281	H	1.998783	2.281253	−0.447169
$5_3^{+\bullet}$				**$5_4^{+\bullet}$**			
C	−2.305132	−0.442095	0.404763	C	0.857761	−0.198104	−2.125970
C	−0.840956	−0.145220	0.797724	C	0.736430	0.030278	−0.593483
C	−2.833462	0.459739	−0.657785	C	2.254776	−0.035831	−2.624630
C	0.096667	−0.354163	−0.422893	C	−0.713518	−0.141523	−0.118135
C	1.498701	0.041326	−0.143065	C	−0.963742	0.051558	1.341737
N	2.493380	−0.819074	−0.175663	N	−0.007109	0.354007	2.184852
O	1.686342	1.301093	0.150776	O	−2.204169	−0.102681	1.718024
H	−2.900949	−0.333220	1.327173	H	0.187641	0.511082	−2.631041
H	−2.405232	−1.493097	0.106934	H	0.486346	−1.206547	−2.352620
H	−0.531740	−0.797495	1.622277	H	1.094473	1.042243	−0.361784

(*contd on next page*)

Appendix A (continued)

H	−0.752894	0.890771	1.142240	H	1.391746	−0.686093	−0.080456
H	−3.474942	0.083997	−1.447064	H	2.933283	−0.880721	−2.668819
H	−2.754995	1.538360	−0.546275	H	2.630936	0.937657	−2.920124
H	0.067193	−1.394012	−0.763253	H	−1.097057	−1.142914	−0.361042
H	3.459529	−0.570422	0.018839	H	−1.388330	0.555347	−0.635767
H	2.317380	−1.789963	−0.412325	H	−0.154224	0.489797	3.181453
H	2.609238	1.554123	0.346428	H	0.943256	0.463173	1.842634
H	−0.271889	0.278213	−1.244003	H	−2.375203	0.022117	2.672299
$1_4^{+\bullet}/5_1^{+\bullet}$				c-**$5^{+\bullet}$**			
C	1.900065	1.157401	−0.311750	C	−0.224789	−1.221121	−0.434615
C	2.088128	−0.337167	−0.038979	C	−1.627495	−0.775994	0.020770
O	−1.084296	1.347129	0.506193	O	0.969560	−0.000612	1.389145
C	−1.323312	0.164798	0.157284	C	0.721463	0.000015	0.037778
C	−0.354539	−0.895776	0.716241	C	−0.224810	1.221557	−0.433539
C	0.828522	−1.205077	−0.217828	C	−1.627707	0.775826	0.020826
N	−2.320824	−0.161809	−0.636550	N	1.947943	0.000358	−0.610696
H	2.868010	1.665701	−0.221344	H	0.152107	−2.142321	0.015798
H	1.507527	1.345327	−1.317735	H	−0.149214	−1.297075	−1.522777
H	1.239312	1.657498	0.410928	H	−1.856462	−1.174397	1.014105
H	2.479451	−0.478376	0.976993	H	−2.374291	−1.196102	−0.660416
H	2.848915	−0.740848	−0.716272	H	0.139252	−0.000530	1.893675
H	−0.997700	−1.775594	0.866081	H	−0.148846	1.298839	−1.521581
H	−0.014631	−0.565338	1.702166	H	0.151863	2.142256	0.018094
H	1.104160	−2.244198	0.026558	H	−1.857540	1.174139	1.013997
H	0.499601	−1.225014	−1.264805	H	−2.374148	1.195738	−0.660870
H	−2.499373	−1.131950	−0.872102	H	2.012094	0.000479	−1.623788
H	−2.948323	0.543353	−1.013962	H	2.813135	−0.000330	−0.071849
$5_1^{+\bullet}$/c-**$5^{+\bullet}$**				**$7_1^{+\bullet}$**			
C	−0.349520	1.337372	−0.200638	C	2.273649	−0.184144	−0.369638
C	−1.726061	0.721247	−0.001928	C	0.922709	0.321854	−0.954558
O	1.927396	0.138057	−0.711293	C	2.357723	−0.055412	1.153156
C	0.794730	−0.104350	−0.008721	C	−0.228807	−0.517068	−0.563279
C	−0.210730	−1.162059	−0.516138	C	−1.444861	−0.022195	−0.014847
C	−1.573248	−0.822486	0.095617	N	−2.449100	−0.840617	0.299160
N	1.084443	−0.129687	1.331229	O	−1.538264	1.280757	0.168860
H	−0.083388	1.605439	−1.224501	H	3.064433	0.406605	−0.843492
H	−0.019608	2.100449	0.502419	H	2.433969	−1.224362	−0.679035
H	−2.344674	0.986636	−0.867423	H	0.999134	0.268861	−2.055637
H	−2.217495	1.126998	0.885701	H	0.753765	1.370509	−0.695124
H	1.785793	0.007955	−1.664391	H	3.342399	−0.373143	1.508848

(*contd on next page*)

Appendix A (continued)

H	0.157225	−2.162938	−0.268692	H	2.208135	0.981460	1.475600
H	−0.245803	−1.073902	−1.608408	H	−0.165118	−1.594351	−0.703697
H	−2.377477	−1.355784	−0.416731	H	−3.329045	−0.517371	0.687175
H	−1.617774	−1.144986	1.143166	H	−2.363726	−1.840055	0.150244
H	0.377344	−0.361667	2.018527	H	−2.384912	1.580551	0.547675
H	1.964569	0.256816	1.662929	H	1.608296	−0.678651	1.657432
$7_2^{+\bullet}$				**$7_3^{+\bullet}$**			
C	2.101065	0.532370	−0.409304	C	−1.077962	−1.112147	−1.300351
C	0.852689	0.744784	0.509283	C	−1.082214	−0.074469	−0.128145
C	2.899915	−0.736089	−0.105511	C	−2.276625	−0.903417	−2.229173
C	−0.171191	−0.311269	0.355170	C	0.033843	−0.303020	0.815875
C	−1.543098	−0.128637	0.017534	C	1.171462	0.536719	1.005749
N	−2.096104	1.063374	−0.188498	N	1.353979	1.678121	0.359090
O	−2.249178	−1.240445	−0.078573	O	2.141023	0.240046	1.853246
H	2.734255	1.414296	−0.263278	H	−1.096502	−2.123290	−0.877602
H	1.777982	0.545416	−1.456623	H	−0.138912	−1.015378	−1.857621
H	0.449077	1.751133	0.347239	H	−2.026547	−0.197451	0.421702
H	1.206701	0.714041	1.553140	H	−1.089100	0.941554	−0.539704
H	3.796008	−0.769020	−0.732620	H	−2.248272	−1.635618	−3.042022
H	3.227997	−0.763127	0.939795	H	−2.269717	0.095400	−2.679441
H	0.111606	−1.349961	0.497758	H	−3.224291	−1.030725	−1.694982
H	2.333204	−1.651400	−0.310269	H	1.989963	−0.601512	2.319555
H	−3.073101	1.185627	−0.431853	H	0.022953	−1.222686	1.398119
H	−1.543408	1.907982	−0.099973	H	2.182887	2.236531	0.540557
H	−3.190439	−1.111993	−0.298279	H	0.680475	2.023966	−0.311893
$1_1^{+\bullet}/7_3^{+\bullet}$				**$5_2^{+\bullet}/7_2^{+\bullet}$**			
C	−1.267617	−1.392147	−1.058501	C	−1.379797	−1.414316	−0.741960
C	−0.718752	−0.059127	−0.520876	C	0.169650	−1.383394	−0.673053
C	−2.225558	−1.181545	−2.234492	C	−1.851369	−1.184357	0.681625
C	0.129005	−0.210218	0.712838	C	0.529336	−0.400543	0.458980
C	1.149772	0.794614	1.089425	C	0.811381	0.987535	0.176952
N	1.111841	2.011929	1.554077	N	0.450748	1.588924	−0.951077
O	2.228781	0.137775	0.807462	O	1.404147	1.658384	1.144541
H	−1.780168	−1.924994	−0.247169	H	−1.751568	−2.362335	−1.146703
H	−0.425877	−2.023287	−1.369778	H	−1.764891	−0.622112	−1.395475
H	−1.562578	0.596053	−0.228848	H	0.644552	−1.136844	−1.629684
H	−0.171863	0.486649	−1.300363	H	0.554414	−2.367239	−0.390128
H	−2.592892	−2.144185	−2.601081	H	−2.703866	−0.535016	0.874886
H	−1.729255	−0.674775	−3.069652	H	−1.757524	−2.015792	1.381679
H	−3.095372	−0.582787	−1.941326	H	1.183147	−0.766389	1.250352

(*contd on next page*)

Appendix A (continued)

H	1.379184	−0.814846	0.444398	H	−0.667201	−0.443383	1.021572
H	−0.238277	−0.812667	1.549993	H	0.623389	2.570556	−1.137151
H	1.970845	2.530490	1.726615	H	0.027700	1.055125	−1.700567
H	0.232019	2.469183	1.768614	H	1.548235	2.604341	0.957164
$5_3^{+\bullet}/7_1^{+\bullet}$				**$11^{+\bullet}$**			
C	−1.951226	1.092651	0.797242	C	−1.947050	−0.008560	−0.963257
C	−1.315855	0.442813	−0.453415	C	−0.905112	−0.310842	0.060838
C	−1.111326	0.611328	1.963447	C	−3.068389	0.907951	−0.452222
C	0.194477	0.518184	−0.178944	C	0.438468	−0.877295	−0.315460
C	1.080862	−0.528650	−0.620544	C	1.573431	−0.162532	0.378579
N	2.370837	−0.313684	−0.864151	N	2.774512	−0.668593	0.483342
O	0.570283	−1.742183	−0.713246	O	1.388455	1.018550	0.885460
H	−3.004600	0.813472	0.911550	H	−2.394106	−0.963974	−1.298058
H	−1.907385	2.184401	0.725277	H	−1.478278	0.416155	−1.862644
H	−1.585153	0.943047	−1.388423	H	−1.219629	−0.445041	1.096834
H	−1.621571	−0.604605	−0.532885	H	0.438043	1.268406	0.767823
H	−0.834119	1.301196	2.758986	H	−3.824776	1.050817	−1.228634
H	−1.250237	−0.420147	2.292587	H	−2.682805	1.894635	−0.173999
H	0.630053	1.513933	−0.286905	H	−3.565557	0.476025	0.422979
H	3.025101	−1.053733	−1.093363	H	0.615576	−0.772635	−1.396454
H	2.750957	0.624119	−0.815298	H	0.519421	−1.953028	−0.092171
H	1.202685	−2.426551	−0.998796	H	3.521690	−0.145097	0.933725
H	0.054549	0.440158	1.135582	H	2.993111	−1.586842	0.112653
$1_1^{+\bullet}/11^{+\bullet}$				**$5_1^{+\bullet}$/6**			
C	−1.821822	0.116639	−0.904329	C	0.204785	−2.426884	0.712764
C	−0.823339	−0.239994	0.160415	C	−1.107206	−2.026062	0.727003
C	−3.005287	0.965769	−0.438547	O	1.330653	0.015336	−0.394227
C	0.440706	−1.027563	−0.243995	C	0.653722	1.112122	−0.286658
C	1.554582	−0.206083	0.346251	C	−0.773932	1.116310	0.181173
N	2.815481	−0.575741	0.398140	C	−1.576622	−0.047326	−0.345789
O	1.195222	0.936341	0.806342	N	1.282283	2.220735	−0.594792
H	−2.196354	−0.866104	−1.269604	H	0.867220	−2.227154	1.552973
H	−1.319640	0.565356	−1.771711	H	0.594122	−3.059811	−0.081652
H	−1.265198	−0.591376	1.100578	H	0.804716	−0.790828	−0.098998
H	−0.285641	0.781453	0.543943	H	−1.533455	−1.601626	1.632357
H	−3.728286	1.084077	−1.249983	H	−1.813602	−2.456200	0.023243
H	−2.676796	1.967597	−0.139715	H	−1.232587	2.078527	−0.093230
H	−3.521791	0.505338	0.410012	H	−0.750062	1.103608	1.282612
H	0.567581	−1.062039	−1.334059	H	−2.609257	−0.071270	−0.011584
H	0.448974	−2.060815	0.119270	H	−1.430922	−0.329422	−1.386073

(*contd on next page*)

Appendix A (continued)

H	3.520729	0.036330	0.799023	H	0.819813	3.121148	−0.553669
H	3.117236	−1.472961	0.035760	H	2.258328	2.196235	−0.879585
$11^{+\bullet}$/12				**$4^{+\bullet}$**			
C	−1.826041	−0.564466	−0.837358	C	1.396498	−0.350408	−0.000029
C	−0.845269	−1.200028	−0.125440	C	0.016193	0.009358	−0.000055
C	−2.322335	1.604769	−0.177983	N	−0.942665	−0.906969	0.000019
C	0.618435	−1.120443	−0.482784	O	−0.236732	1.297219	−0.000024
C	1.317170	−0.041722	0.308726	H	1.704436	−1.389542	0.000002
N	2.584970	−0.097312	0.627730	H	2.138838	0.438773	0.000258
O	0.663286	1.013300	0.687642	H	−1.932336	−0.676855	−0.000084
H	−2.864101	−0.779320	−0.608737	H	−0.712420	−1.895917	0.000129
H	−1.627630	−0.179309	−1.834719	H	−1.182157	1.540872	0.000253
H	−1.092963	−1.733136	0.789461	**8^{+}**			
H	−0.290765	0.932018	0.430211	C	−0.832638	−0.677306	−0.000056
H	−3.244685	1.587520	−0.749399	C	0.451910	−0.006562	−0.000015
H	−1.557829	2.274020	−0.570481	N	1.575357	−0.698985	0.000041
H	−2.442135	1.560178	0.902158	O	0.449156	1.303134	−0.000039
H	0.747388	−0.853976	−1.543063	C	−1.989965	0.004902	0.000047
H	1.134932	−2.074477	−0.327488	H	−0.813295	−1.762973	−0.000164
H	3.025504	0.662588	1.140991	H	2.496136	−0.270992	0.000046
H	3.159440	−0.889976	0.364857	H	1.551923	−1.713694	0.000072
$6^{+\bullet}$				H	1.330409	1.721631	0.000037
C	−0.918767	−0.204001	0.655674	H	−2.023154	1.090134	0.000161
C	0.476770	0.014473	0.138493	H	−2.938603	−0.522486	0.000025
N	1.266671	−0.984268	−0.183151	**10^{+}**			
O	0.824388	1.261946	−0.015162	C	−1.897568	0.220879	−0.248739
C	−1.866684	−0.018732	−0.497604	C	−0.815238	−0.653186	0.297014
H	−0.996068	−1.205053	1.091545	C	0.585159	−0.055563	0.037085
H	−1.096391	0.537520	1.443090	N	0.823948	1.228453	0.104608
H	2.186430	−0.862903	−0.599711	O	1.450034	−0.937749	−0.221459
H	0.966896	−1.942076	−0.029514	H	−2.851308	0.206894	0.272411
H	1.704032	1.410766	−0.414629	H	−1.866950	0.589514	−1.268887
H	−2.192319	−0.871359	−1.081741	H	−0.837255	−1.670125	−0.128214
H	−2.182291	0.976977	−0.785069	H	−0.857611	−0.775073	1.389506
9^{+}				H	1.754805	1.612817	−0.039100
C	1.507124	−0.187685	0.000015	H	0.056289	1.866011	0.301543
C	0.595281	1.066572	−0.000006	**13^{+}**			
C	−0.489368	0.035299	−0.000008	C	−1.197429	0.048194	0.082744
N	−1.790413	0.023661	0.000010	C	−0.501573	−1.262659	0.516186
O	0.258355	−1.035056	−0.000013	C	0.126841	0.682273	−0.266844

(*contd on next page*)

Appendix A (continued)

H	2.073954	−0.393119	−0.906398	O	0.647810	1.641795	−0.671223
H	2.073903	−0.393119	0.906460	N	0.888411	−0.722383	0.196717
H	0.634230	1.692575	−0.895716	H	−1.721966	0.601652	0.869823
H	0.634214	1.692614	0.895677	H	−1.861348	−0.020078	−0.786470
H	−2.303913	−0.856088	0.000004	H	−0.584033	−1.509627	1.573804
H	−2.324561	0.886835	0.000005	H	−0.724173	−2.135824	−0.095688
12^{+}				H	1.396713	−1.201615	−0.555907
C	−0.305524	−0.457729	0.788348	H	1.526415	−0.619033	0.994682
C	0.935199	0.062318	0.130465	**14**$^{+}$			
N	1.869549	−0.740209	−0.324384	C	1.448421	−0.052068	−0.681047
O	1.001663	1.356696	−0.000303	C	1.446194	−0.052618	0.681550
C	−1.423987	−0.547586	−0.243379	C	−0.703600	0.164171	0.000378
C	−2.460869	0.288112	−0.265831	N	−1.177203	−1.057811	−0.000771
H	−0.098000	−1.435279	1.238261	O	−1.011410	1.287867	−0.000111
H	−0.573798	0.242055	1.584981	H	1.518862	−0.973503	−1.255620
H	2.695685	−0.418835	−0.822741	H	1.466174	0.877665	−1.244561
H	1.789556	−1.743199	−0.188071	H	1.463131	0.876517	1.246259
H	1.784076	1.694723	−0.478803	H	1.515806	−0.974702	1.255213
H	−1.342039	−1.355844	−0.967221	H	−2.190089	−1.181052	−0.002914
H	−3.252522	0.174103	−1.000277	H	−0.588280	−1.880095	0.002620
H	−2.572018	1.099483	0.449375				

References

[1] J. Loos, D. Schröder, W. Zummack, H. Schwarz, R. Thissen, O. Dutuit, Int. J. Mass Spectrom. 214 (2002) 105.

[2] D. Schröder, J. Loos, M. Semialjac, T. Weiske, H. Schwarz, G. Höhne, R. Thissen, O. Dutuit, Int. J. Mass Spectrom. 214 (2002) 155.

[3] M.J. Frisch, G.W. Trucks, H.B. Schlegel, G.E. Scuseria, M.A. Robb, J.R. Cheeseman, V.G. Zakrzewski, J.A., Montgomery Jr., R.E. Stratmann, J.C. Burant, S. Dapprich, J.M. Millam, A.D. Daniels, K.N. Kudin, M.C. Strain, O. Farkas, J. Tomasi, V. Barone, M. Cossi, R. Cammi, B. Mennucci, C. Pomelli, C. Adamo, S. Clifford, J. Ochterski, G.A. Petersson, P.Y. Ayala, Q. Cui, K. Morokuma, D.K. Malick, A.D. Rabuck, K. Raghavachari, J.B. Foresman, J. Cioslowski, J.V. Ortiz, A.G. Baboul, B.B. Stefanov, G. Liu, A. Liashenko, P. Piskorz, I. Komaromi, R. Gomperts, R.L. Martin, D.J. Fox, T. Keith, M.A. Al-Laham, C.Y. Peng, A. Nanayakkara, C. Gonzalez, M. Challacombe, P.M.W. Gill, B. Johnson, W. Chen, M.W. Wong, J.L. Andres, C. Gonzalez, M. Head-Gordon, E.S. Replogle, J.A. Pople, GAUSSIAN 98, Revision A.7, Gaussian, Inc., Pittsburgh, PA, 1998.

[4] A.D. Becke, J. Chem. Phys. 98 (1993) 1372, 5648.

[5] C. Lee, W. Yang, R.G. Parr, Phys. Rev. B 37 (1988) 785.

[6] W. Koch, M.C. Holthausen, A Chemist's Guide to Density Functional Theory, Wiley, Weinheim, 2000.

[7] A.P. Scott, L. Radom, J. Phys. Chem. 100 (1996) 16502.

[8] M.W. Wong, Chem. Phys. Lett. 256 (1996) 391.

[9] Spartan 3.1, Wavefunction Inc., Irvine, USA, 1994.

[10] R.D. Brown, P.D. Godfey, B. Kleibömer, J. Mol. Spectrosc. 124 (1987) 34.

[11] K.-M. Marstokk, H. Møllendal, S. Samdal, J. Mol. Struct. 376 (1996) 11.

[12] (a) E.D. Stevens, Acta Cryst. B 34 (1978) 544;
(b) H. Ohtaki, A. Funaki, B.M. Rode, G.J. Reibnegger, Bull. Chem. Soc. Jpn. 56 (1983) 2116;
(c) L.P. Olson, Y. Li, K.H. Houk, A.J. Kresge, L.J. Schaad, J. Am. Chem. Soc. 117 (1995) 2992.

[13] (a) E.D. Stevens, Acta Cryst. B 34 (1978) 544;
(b) H. Ohtaki, A. Funaki, B.M. Rode, G.J. Reibnegger, Bull. Chem. Soc. Jpn. 56 (1983) 2116;
(c) L.P. Olson, Y. Li, K.H. Houk, A.J. Kresge, L.J. Schaad, J. Am. Chem. Soc. 117 (1995) 2992.

[14] (a) E.D. Stevens, Acta Cryst. B 34 (1978) 544;
(b) H. Ohtaki, A. Funaki, B.M. Rode, G.J. Reibnegger, Bull. Chem. Soc. Jpn. 56 (1983) 2116;
(c) L.P. Olson, Y. Li, K.H. Houk, A.J. Kresge, L.J. Schaad, J. Am. Chem. Soc. 117 (1995) 2992.

[15] (a) Y. Sugawara, Y. Hamada, A.Y. Hirakawa, M. Tsuboi, S. Kato, K. Morokuma, Chem. Phys. 50 (1980) 105;
(b) G.M. Wright, R.J. Simmonds, D.E. Parry, J. Comput. Chem. 9/6 (1988) 600;
(c) X.-C. Wang, J. Nichols, M. Feyereisen, M. Gutowski, J. Boatz, A.D.J. Haymet, J. Simons, J. Phys. Chem. 95 (1991) 10419;
(d) F. Sim, A. St-Amant, I. Papai, D.R. Salahub, J. Am. Chem. Soc. 114 (1992) 4391;
(e) G. Dive, D. Dehareng, J.M. Ghuysen, S.-Y. Chu, Theor. Chim. Acta 85 (1993) 409;
(f) M.-C. Ou, J. Phys. Chem. 99 (1995) 556.
[16] I.N. Demetropoulos, I.P. Gerothanassis, C. Vakka, C. Kakavas, J. Chem. Soc., Faraday Trans. 92 (1996) 921.
[17] S. Samdal, J. Mol. Struct. 440 (1998) 165.
[18] T. Helgaker, J. Gauss, P. Jørgensen, J. Olsen, J. Chem. Phys. 106 (1997) 6430.
[19] M.W. Wong, K.B. Wiberg, J. Phys. Chem. 96 (1992) 668.
[20] R.R. Parr, R.G. Yang, Density Functional Theory of Atoms and Molecules, Oxford University Press, New York, 1989.
[21] (a) P. Hobza, J. Sponer, T. Reschel, J. Comput. Chem. 16–19 (1995) 1315;
(b) J.J. Novoa, C. Sosa, J. Phys. Chem. 99 (1995) 15837.
[22] D.J. Henry, L. Radom, in: J. Cioslowski (Ed.), Quantum-Mechanical Prediction of Thermochemical Data, Kluwer, Dordrecht, 2001, p. 161.
[23] J. Loos, Diplomarbeit, TU, Berlin, 2000.
[24] L.A. Curtiss, P.C. Redfern, K. Raghavachari, J.A. Pople, J. Chem. Phys. 109 (1998) 42.
[25] D. Schröder, J. Loos, H. Schwarz, R. Thissen, D.V. Preda, L.T. Scott, D. Caraiman, M.V. Frach, D.K. Böhme, Helv. Chim. Acta 84 (2001) 1625.
[26] (a) M.J. Frisch, K. Raghavachari, J.A. Pople, W.J. Bouma, L. Radom, Chem. Phys. 75 (1983) 323;
(b) B.F. Yates, R.H. Nobes, L. Radom, Chem. Phys. Lett. 116 (1985) 474;
(c) N. Heinrich, H. Schwarz, in: J.P. Maier (Ed.), Ion and Cluster-Ion Spectroscopy and Structure, Elsevier, Amsterdam, 1989, p. 329.
[27] N. Heinrich, W. Koch, G. Frenking, H. Schwarz, J. Am. Chem. Soc. 108 (1986) 593.
[28] (a) C.-C. Wu, M.H. Lien, J. Phys. Chem. 100 (1996) 594;
(b) K. Sung, T.T. Tidwell, J. Am. Chem. Soc. 120 (1998) 3043;
(c) S. Sklenak, Y. Apeloig, Z. Rappoport, J. Am. Chem. Soc. 120 (1998) 10359;
(d) R.E. Rosenberg, J. Org. Chem. 63 (1998) 5562; (e) G. Raspoet, M.T. Nguyen, S. Kelly, A.F. Hegarty, J. Org. Chem. 63 (1998) 9669.
[29] C.K. Lin, S.Y. Chen, M.H. Lien, J. Phys. Chem. 99 (1995) 1454.
[30] (a) S.G. Lias, J.E. Bartmess, J.F. Liebman, J.L. Holmes, R.D. Levin, W.G. Mallard, J. Phys. Chem. Ref. Data 17 (Suppl. 1) (1988).;
(b) NIST Chemistry WebBook, NIST Standard Reference Database Number 69, P.J. Linstrom, W.G. Mallard (Eds.) July 2001, National Institute of Standards and Technology, Gaithersburg, MD, 20899, USA. Available: http://webbook.nist.gov.
[31] P. Mourgues, J. Chamot-Rooke, H. Nedev, H.-E. Audier, J. Mass Spectrom. 36 (2001) 102.
[32] E.P.L. Hunter, S.G. Lias, J. Phys. Ref. Data 27 (1998) 413.
[33] J. Berkowitz, G.B. Ellison, D. Gutman, J. Phys. Chem. 98 (1994) 2744.